

1 **Activation of Ca²⁺ phosphatase Calcineurin regulates Parkin translocation to mitochondria and**
2 **mitophagy**

3 **Elena Marchesan¹, Alice Nardin^{1,2}, Sofia Mauri¹, Simone Di Paola^{3,4}, Monica Chinellato¹, Sophia**
4 **von Stockum¹, Joy Chakraborty¹, Stephanie Herkenne¹, Valentina Basso¹, Emilie Schrepfer^{1,5},**
5 **Oriano Marin⁶, Laura Cendron¹, Diego L. Medina^{3,7}, Luca Scorrano^{1,5} and Elena Ziviani^{1*}**

6 ¹Department of Biology, University of Padova, Padova, Italy.

7 ²Medical Research Council Protein Phosphorylation and Ubiquitylation Unit, University of Dundee,
8 Dundee, UK

9 ³Telethon Institute of Genetics and Medicine (TIGEM), Pozzuoli, Naples, Italy.

10 ⁴current address: Institute for Experimental Endocrinology and Oncology (IEOS), National Research
11 Council (CNR), Napoli, Italy

12 ⁵Dulbecco-Telethon Institute, Venetian Institute of Molecular Medicine (VIMM), Padova, Italy

13 ⁶ Department of Biomedical Sciences (DSB), University of Padova, Padova, Italy.

14 ⁷Medical Genetics Unit, Department of Medical and Translational Science, Federico II University,
15 Naples, Italy

16

17 *Correspondence should be addressed to E.Z. (e-mail elena.ziviani@unipd.it)

18

19 **Abstract**

20 Selective removal of dysfunctional mitochondria via autophagy is crucial for the maintenance of
21 cellular homeostasis. This event is initiated by the translocation of the E3 ubiquitin ligase Parkin to
22 damaged mitochondria, and it requires the Serine/Threonine-protein kinase PINK1. In a
23 coordinated set of events, PINK1 operates upstream of Parkin in a linear pathway that leads to the
24 phosphorylation of Parkin, Ubiquitin, and Parkin mitochondrial substrates, to promote
25 ubiquitination of outer mitochondrial membrane proteins. Ubiquitin decorated mitochondria are
26 selectively recruiting autophagy receptors, which are required to terminate the organelle via
27 autophagy. In this work we show a previously uncharacterized molecular pathway that correlates
28 the activation of the Ca²⁺-dependent phosphatase Calcineurin to Parkin-dependent mitophagy.
29 Calcineurin downregulation or genetic inhibition prevents Parkin translocation to CCCP-treated
30 mitochondria, and impairs stress-induced mitophagy, whereas Calcineurin activation promotes
31 Parkin mitochondrial recruitment and basal mitophagy. Calcineurin interacts with Parkin, and
32 promotes Parkin translocation in the absence of PINK1, but requires PINK1 expression to execute
33 mitophagy in MEF cells. Genetic activation of Calcineurin *in vivo* boosts basal mitophagy in
34 neurons, and corrects locomotor dysfunction and mitochondrial respiratory defects of a
35 *Drosophila* model of impaired mitochondrial functions.
36 Our study identifies Calcineurin as a novel key player in the regulation of Parkin translocation and
37 mitophagy.

38

39

40 Introduction

41 The Ubiquitin Proteasome System (UPS) and mitophagy are dysregulated in many neurological
42 diseases, including Parkinson's Disease (PD), a neurodegenerative condition characterized by
43 dopaminergic neuron loss^{1,2}, accumulation of ubiquitinated unfolded protein aggregates^{3,4},
44 mitochondrial dysfunction and mitophagy dysregulation^{5,6}. Although most PD cases are sporadic, a
45 small proportion derives from mutations in PD associated genes^{7,8}, which have been identified by
46 characterizing familiar Mendelian inherited PD forms, and includes mutations in the mitophagy
47 genes PINK1 and Parkin⁹⁻¹¹. Parkin belongs to the RBR (RING-between-RING) type of E3 ubiquitin
48 ligases¹², also known as RING/HECT hybrids, consisting of an ubiquitin like domain (Ubl), followed
49 by two RING fingers domains (RING0 and RING1), an in between RING finger domain (IBR), a linker
50 domain called Repressor Element of Parkin (REP) and a third RING finger domain called RING2¹³⁻¹⁶.
51 Under basal conditions, Parkin activity is repressed and the protein maintains a close structure
52 with the Ubl domain and the REP fragment occluding the RING1 domain, and the RING0 domain
53 impeding on the catalytic site-containing RING2 domain¹⁴⁻¹⁶. The gene product has a number of
54 neuroprotective roles and pleiotropic functions and its activation is involved in many different
55 survival pathways¹⁷⁻¹⁹, including those that are affecting mitochondrial function by regulating
56 mitochondria quality control²⁰⁻²⁴. How Parkin controls so many different cellular processes is under
57 intense investigation. However, by being a versatile E3 ubiquitin ligase that both promotes
58 degradative Lys 48-mediated ubiquitination and nonclassical, proteosomal-independent
59 ubiquitination²⁵⁻³¹, Parkin has the potential of controlling a broad subset of cellular processes. Not
60 surprisingly, Parkin activity is repressed under basal conditions, and its activation is tightly
61 regulated by a number of molecular processes, which are largely mediated by post translational
62 modifications^{13,14,16}. Parkin function is closely related to the activity of another PD-related gene,
63 PARK6, which encodes for a protein called PINK1³²⁻³⁴. PINK1 is a Serine/Threonine kinase that is
64 imported into mitochondria, where it gets cleaved by the inner membrane protease PARL and
65 then eliminated by the proteasome³⁵⁻³⁷. On depolarized mitochondria, PINK1 accumulates on the
66 outer mitochondrial membrane (OMM), where it promotes Parkin translocation and mitochondrial
67 recruitment^{33,34,38,39}. Independent studies showed that PINK1-mediated phosphorylation of Parkin
68 and Ubiquitin at residue Serine 65 (Ser65) is required for Parkin translocation to defective
69 mitochondria, and for its E3-ubiquitin ligase activity⁴⁰⁻⁴³. This process leads to Parkin-dependent
70 ubiquitination and proteasomal degradation of OMM proteins, and to the selective autophagy of
71 damaged mitochondria⁴⁴⁻⁴⁸. Moreover, PINK1 phosphorylates a number of Parkin substrates

72 including the pro-fusion protein Mitofusin, Mfn2, which work as Parkin receptor⁴⁹. It was proposed
73 that Parkin-dependent ubiquitination of Mitofusins prevents mitochondrial fusion of dysfunctional
74 mitochondria by promoting proteasomal degradation of Mfn1 and Mfn2²⁴, and segregates
75 depolarized mitochondria from the mitochondrial network, impairing their ability to refuse⁵⁰. In
76 addition, PINK1 directly promotes mitochondrial fission by regulating recruitment and activation
77 of pro-fission protein Drp1⁵¹. In resting conditions, Drp1 is phospho-inhibited at Ser 637 by AKAP1-
78 PKA (A-kinase anchoring protein complex and protein kinase A, respectively)⁵². Following
79 mitochondria damage, PINK1 becomes active and disrupts the AKAP1-PKA complex to promote
80 Drp1-dependent fission⁵¹. Moreover, PINK1 directly phosphorylates Drp1 on Ser 616 to regulate
81 mitochondrial fission⁵³. Interestingly, Drp1 is selectively recruited to dysfunctional mitochondria in
82 the proximity of PINK1/Parkin suggesting that mitochondrial division occurs at sites where the
83 PINK1/Parkin-dependent mitochondrial clearance program is initiated⁵⁴. Expression of dominant-
84 negative Drp1 to inhibit mitochondrial fission prevents mitophagy, indicating the importance of
85 fission in mitophagy⁵⁵, which is also supported by studies on yeasts⁵⁶. Translocation of Drp1 to
86 mitochondria is mediated by selective dephosphorylation of residue Serine 637, which is
87 controlled by Ca²⁺ and Ca²⁺/Calmodulin dependent phosphatase Calcineurin (CaN)⁵². Rise of
88 cytosolic Ca²⁺ associated to mitochondrial depolarization⁵⁷, leads to CaN-dependent Drp1
89 dephosphorylation and Drp1 mitochondrial recruitment to promote mitochondrial fission⁵², which
90 is required to execute mitophagy^{58,59}. CaN also dephosphorylates transcription factor TFEB to
91 promote its nuclear translocation and the expression of autophagy and lysosomal genes to induce
92 autophagy and lysosomal biogenesis⁶⁰.

93 In this work, we show that Ca²⁺/Calmodulin phosphatase CaN is required for Parkin mitochondrial
94 recruitment and mitophagy in CCCP-treated mouse embryonic fibroblast cells (MEFs). CaN
95 activation is sufficient to promote Parkin translocation under basal condition in a PINK1-
96 independent fashion. Genetic activation of CaN *in vivo* promotes basal mitophagy in neurons, and
97 corrects locomotor dysfunction and mitochondrial defects of a *Drosophila* model of impaired
98 mitochondrial function.

99

100 **Results**

101 **Parkin translocation to mitochondria is regulated by Calcineurin**

102 We transfected mouse embryonic fibroblasts (MEFs), , with fluorescent mCherry-Parkin and
103 mitochondrial targeted YFP (mitoYFP), and analyzed Parkin subcellular localization by confocal
104 microscopy, following established experimental protocols^{34,38,46}. Consistent with previous
105 studies^{33,38,46,61}, we observed that mCherry-Parkin was predominantly located in the cytosol in
106 non-treated cells (Figure 1A, upper panel). Following the treatment with uncoupling agent
107 carbonyl cyanide m-chlorophenylhydrazone (CCCP), a significant proportion of cells (75,7±1,9%)
108 showed mCherry-Parkin accumulated on or near fragmented mitochondria (Figure 1A, lower
109 panel), forming discrete dots, which we called puncta (quantified in Figure 1B). An automated
110 analysis of the confocal images with Squassh, an ImageJ plugin that calculates the degree of
111 colocalization between two channels⁶², allowed to further consolidate this result. In this analysis,
112 the colocalization coefficient computed by the Squassh plugin ranges from 0 to 1, where 0
113 indicates no colocalization, and 1 perfect colocalization between mCherry-Parkin and YFP labeled
114 mitochondria. According to this analysis, Squassh index raised from 0,29±0,03 to 0,62±0,06
115 following CCCP treatment, indicative of increased Parkin mitochondrial recruitment (Figure 1C). A
116 small proportion of Parkin puncta did not seem to colocalize with mitochondria (Figure 1A,
117 arrowhead) suggesting a potential recruitment of Parkin to other organelles. To test this
118 hypothesis, we cotransfected mCherry-Parkin expressing MEFs with the lysosomal marker
119 LAMP1GFP or the endosomal marker Rab5BGFP. Colocalization analysis using Squassh
120 demonstrated that in CCCP-treated cells a small proportion of Parkin puncta colocalized with
121 lysosomes (Figure 1D, quantified in Figure 1E), whether no significant recruitment to endosomes
122 occurs (Figure 1F; quantified in Figure 1G). The addition of the protophore CCCP, required for
123 triggering Parkin translocation, induces a transient increase of Ca²⁺ influx⁵⁷. Importantly, Ca²⁺
124 chelation with BAPTA abolishes Parkin translocation (Supplementary Figure 1), indicating a role for
125 Ca²⁺-dependent signal in the regulation of Parkin mitochondrial recruitment. Because
126 mitochondria need to fragment to be engulfed by the autophagosome^{58,59}, and rise of cytosolic
127 Ca²⁺ associated to mitochondrial depolarization leads to Calcineurin (CaN)-dependent Drp1
128 fission⁵² and autophagy⁶⁰, it is conceivable that CaN may also play a role in Parkin recruitment and
129 Parkin-dependent mitophagy. Treatment with FK506, an immunosuppressive agent that blocks
130 CaN without affecting the permeability transition pore (PTP)⁶³, impaired Parkin translocation
131 (Supplementary Figure 2). This was also the case upon addition of smaller concentration of CCCP,

132 and following treatment with other mitochondrial damaging compounds that promoted
133 mitochondrial depolarization (Supplementary Figure 3). To further support this result, we took
134 advantage of the existing dominant negative mutant of CaN ($\Delta\text{CnA}^{\text{H151Q}}$)^{64,65}. CaN is a heterodimer,
135 composed of a catalytic subunit (CnA) that binds calmodulin and a regulatory subunit (CnB) that
136 binds Ca^{2+} . Ca^{2+} /calmodulin activates CaN upon binding to the calmodulin-binding domain of CnA
137 and inducing the dissociation of the autoinhibitory domain from the catalytic domain⁵². $\Delta\text{CnA}^{\text{H151Q}}$
138 dominant negative mutant misses the calmodulin binding domain and the autoinhibitory domain
139 and harbors an inactivating His-151 to Gln point mutation. We cotransfected MEFs with mCherry-
140 Parkin and dominant negative CaN (CnB plus $\Delta\text{CnA}^{\text{H151Q}}$) and looked at Parkin localization. As
141 previously showed, CCCP-induced Parkin mitochondrial recruitment was clearly visible following
142 3hrs CCCP (Figure 2A, left panel). This event was completely abolished when in presence of the
143 dominant negative CaN, $\Delta\text{CnA}^{\text{H151Q}}$ (Figure 2A, right panel; quantified in Figure 2B-C). CaN
144 downregulating cells (Supplementary Figure 4) also exhibited a significant decrease in Parkin
145 recruitment upon CCCP treatment (Figure 2D, quantified in Figure 2E-F).

146 **Parkin translocation is induced by Calcineurin in the absence of PINK1**

147 Parkin translocation and activity are strictly controlled by mechanisms of autoinhibition that can
148 be released by PINK1^{13,15,16,66-68}. The current model for the mechanism of Parkin activation and
149 recruitment by PINK1 depicts that under basal conditions Parkin activity is repressed and the
150 protein maintains a close structure with the ubiquitin-like domain (UBL) and the repressor
151 element of Parkin (REP) fragment occluding the RING1 domain and the RING0 domain impeding on
152 the catalytic site-containing RING2 domain¹⁴⁻¹⁶. Structural studies have provided evidence that
153 phosphorylation of Ubiquitin and Parkin at Serine 65 by PINK1 causes displacement of the
154 inhibitory UBL and stretches the REP⁴³. This affects Parkin autoinhibitory structure and contributes
155 to promote Parkin conformational change that leads to Parkin mitochondrial recruitment and
156 activation^{43,69,70}. In line with this model and as already reported^{38,39}, we found that Parkin does not
157 translocate to CCCP-treated mitochondria in the absence of PINK1 (Figure 3A, left panel).
158 Intriguingly, expression of constitutive active CaN (CnB plus ΔCnA) promoted Parkin translocation
159 in PINK1 KO cells, even in the absence of CCCP (Figure 3A, right panel; quantified in Figure 3B-C), a
160 condition that was hold true also in PINK1 wild-type cells (Supplementary Figure 5). Moreover, in
161 PINK1 KO MEFs transfected with phospho-mimetic Ub (Ub S65E), a large proportion of phospho-
162 mimetic mCherry-Parkin (Parkin S65E) translocated to CCCP-treated mitochondria (Figure 3D, left
163 panel), a condition that was abolished upon expression of CaN dominant negative $\Delta\text{CnA}^{\text{H151Q}}$

164 (Figure 3D, right panel; quantified in Figure 3E-F). Based on these results, it is expected that
165 expression of CaN can affect Parkin conformational change in the absence of PINK1 to promote
166 Parkin translocation. Because conformational changes are paralleled by changes in protein
167 solubility, which can be assessed by thermal shift^{71,72}, we performed a thermal stability assay for
168 Parkin to test this hypothesis. Expression of constitutive active CaN leads to a decrease in Parkin
169 thermal stability in wild type (Figure 3G-H) and PINK1 KO cells (Figure 3I-J), supporting the
170 hypothesis that Parkin undergoes a conformational change in this condition regardless PINK1
171 expression.

172 Thus, expression of constitutively active CaN promotes Parkin recruitment in PINK1 KO cells that is
173 in the absence of PINK1-dependent phosphorylation of Parkin and Ubiquitin.

174 **Calcineurin interacts with Parkin**

175 Our results prompted us to evaluate the possibility of an interaction between CaN and Parkin. To
176 evaluate this possibility, we first performed an *in vitro* interaction assay by generating affinity-
177 purified recombinant His-tagged Parkin from bacteria, which was coupled to a His-affinity resin
178 and incubated with protein lysate extracted from cells expressing Flag-tagged CaN. The resin was
179 washed to remove nonspecifically adhering proteins, and Laemmli buffer was used to elute the
180 complexes from the resin (Figure 4A). Importantly, in the eluted complexes we were able to
181 identify CaN (Figure 4B), indicating that CaN binds to Parkin *in vitro*. The interaction was specific
182 for CaN because an unrelated Flag-tagged protein that is not supposed to interact with Parkin
183 (USP14-Flag) was not retrieved in the eluted complexes when protein lysate from cells expressing
184 USP14-Flag was incubated with the resin. Likewise, no interaction was retrieved when His-tagged
185 MEF2D, which does not interact with CaN, was used as a bait to retrieve CaN (Figure 4B).

186 We next performed a proximity ligation assay (PLA) to investigate Parkin and CaN interaction *in*
187 *situ*. We were able to visualize discrete spots (PLA signal) in HeLa cells co-expressing mCherry-
188 Parkin and CaN-Flag, representative of Parkin-CaN close proximity. In this assay, the interaction
189 between GRASP65 and Parkin was used as negative biological control, whereas the interaction
190 between GRASP65 and GM130 was used as positive control for PLA^{73,74}. PLA detection dots
191 indicate positive interaction (Figure 4C; quantified in Figure 4D). The specificities of the antibodies
192 used in the PLA were tested by immunofluorescence (Supplementary Figure 6).

193 Finally, to evaluate the possibility of an interaction at the endogenous level, we performed an
194 immunoprecipitation (IP) assay in HEK 293T cells, which express relatively high levels of
195 endogenous Parkin. HEK cells were treated with DMSO or CCCP for 2hrs, and endogenous Parkin

196 from cell lysate was captured by specific Parkin antibody. The antibody-protein complexes were
197 pulled out of the sample using Protein A-coupled agarose beads. Endogenous CaN co-
198 immunoprecipitated with Parkin in these complexes, indicating that endogenous CaN and Parkin
199 interact. Notably, the interaction between endogenous Parkin and CaN was detectable only upon
200 CCCP treatment to activate CaN, and not under basal conditions (Figure 4E). To further strengthen
201 this result, we also performed the reverse IP, i.e. we pulled down endogenous CaN from lysate of
202 cells treated with CCCP as before, and we were able to retrieve endogenous Parkin from the
203 pulled down sample (Supplementary Figure 7).

204 Thus, CaN interacts with Parkin.

205 **Parkin translocation is induced by Calcineurin independently of Drp1 mitochondrial recruitment** 206 **and activity**

207 Previous reports demonstrated that CaN regulates the phosphorylation status of mitochondrial
208 pro fission protein Drp1, and that dephosphorylation by CaN on Serine 637 is required for Drp1
209 translocation and in the process of mitochondrial fission⁵². Because CaN activation promotes
210 mitochondrial recruitment of Drp1 and Parkin, we addressed whether these two events were
211 correlated. Interestingly, expression of constitutive dephosphorylated Drp1 (Drp1 S637A) that was
212 shown to be mostly mitochondrial and to promote mitochondrial fragmentation⁵², did not affect
213 Parkin translocation in presence of CaN dominant negative (Figure 5A-B). Moreover, promotion of
214 Parkin recruitment by expression of constitutive active CaN was not inhibited in presence of Drp1
215 dominant negative (Drp1 K38A) (Figure 5C-D), indicating that Parkin translocation is independent
216 of Drp1 recruitment to the mitochondria to drive mitochondrial fragmentation.

217 **Calcineurin is required for CCCP-induced mitophagy**

218 Our data demonstrate that CaN interacts with Parkin, and that CaN activity is required for Parkin
219 recruitment to mitochondria. What about mitophagy? We used four different approaches to
220 evaluate mitophagy *in vitro* in MEFs, namely (i) quantification of mitochondrial mass, estimated by
221 western blotting analysis of inner mitochondrial membrane protein ATP synthase (ATP5A), (ii)
222 confocal analysis of LC3-decorated mitochondria, (iii) FACS and confocal analysis of mitochondria-
223 targeted fluorescent probe mt-Keima, and (iv) electron microscopy (EM).

224 Because MEFs have negligible levels of Parkin^{44,75-77}, which might affect our ability to investigate
225 Parkin-dependent events, we utilized a well established experimental system^{34,46,78-80} in which we
226 introduced exogenous Parkin into MEFs by generating a Parkin-flag stable cell line by retroviral
227 infection⁸¹. MEFs stably expressing Parkin-flag were transfected with dominant negative CaN

228 ($\Delta\text{CaN}^{\text{H151Q}}$) or corresponding empty vectors, and mitochondrial mass was assessed following
229 treatment with CCCP. In this condition, mitochondrial protein ATP synthase subunit alpha, ATP5A
230 was lost after 36 hrs CCCP treatment, while it was retained in cells expressing dominant negative
231 CaN, $\Delta\text{CaN}^{\text{H151Q}}$ (Figure 6A-B). Cells downregulating CaN also exhibited impaired CCCP-induced
232 mitochondrial degradation (Figure 6C-D). These quantitative immunoblotting data were confirmed
233 by confocal analysis of colocalization of mito-Kate labelled mitochondria with GFP-LC3 labelled
234 autophagosomes. Cells expressing dominant negative CaN (Figure 6E) or downregulating CaN
235 (Figure 6F) presented impaired LC3-mitochondria colocalization, following CCCP (quantified in
236 Figure 6G-H). To further evaluate mitophagy in our model system, we infected Parkin expressing
237 MEFs with mt-Keima, a pH-dependent fluorescence probe targeted to the mitochondrial matrix,
238 which has different excitation spectra at neutral and acidic pH⁸². Keima has a single emission peak
239 at 620 nm with a bimodal excitation spectrum. These properties of mt-Keima allow rapid FACS
240 determination of “acidic” mitochondria undergoing autolysosome degradation. The mt-Keima
241 assay showed that CCCP-induced mitophagy was greatly reduced in cells downregulating CaN, in
242 line with the results obtained with the biochemical approaches (Figure 6I and Supplementary
243 Figure 8).

244 **Constitutive active Calcineurin induces an increase in basal mitophagy**

245 We previously demonstrated that the expression of constitutive active CaN promotes Parkin
246 translocation even in absence of CCCP treatment. To address whether this was also the case for
247 mitophagy, we performed mt-Keima assay in Parkin expressing MEFs transiently transfected with
248 constitutively active CaN. Representative image of mt-Keima acquired at confocal microscope
249 clearly showed increased number of red fluorescence in control cells expressing constitutively
250 active CaN, ΔCaN (Figure 7A). In these cells basal mitophagy (i.e. untreated cells) was increased
251 (Figure 7B). Qualitative electron microscopy demonstrated an increase in autophagosomes and
252 autolysosomes with mitochondrial like-structures inside in this condition (Figure 7C-D).

253 **Calcineurin requires PINK1 and mitochondrial fission to promote mitophagy in MEFs**

254 While investigating Parkin translocation in PINK1 KO background, we came across the unexpected
255 finding that expression of constitutive active CaN triggered Parkin translocation in the absence of
256 PINK1 (Figure 3). Parkin translocation induced by CaN is independent of Drp1 activity and Drp1
257 mitochondrial recruitment to promote mitochondrial fission (Figure 5). Based on these
258 observations, we now want to address the potential “mitophagic” effect of CaN activation in
259 PINK1 KO background. Importantly, expression of constitutive active CaN in PINK1 KO cells failed

260 to promote the degradation of mitochondrial protein ATP5A (Figure 8A-B). These quantitative
261 immunoblotting results were confirmed by mt-Keima assay (Figure 8C). Analysis of protein levels
262 of *bona-fide* Parkin substrates⁴⁸ revealed that the levels of TOM20, Mfn1 and VDAC were
263 decreased when constitutive active CaN was expressed in WT and PINK1 KO background (Figure
264 8D-E). In this condition, we also tracked an increase in the coefficient of colocalization between
265 Ubiquitin and TOM20 (Figure 8F-G). Importantly, in MEFs that do not stably express Parkin,
266 expression of constitutive active CaN failed to enhance mitophagy (Supplementary figure 9)
267 further supporting the hypothesis that CaN-induced mitophagy is mediated by Parkin and not
268 other E3 ubiquitin ligases that are known to share common mitochondrial targets (for example
269 MARCH5⁸³ and/or Mul1⁸⁴). Of note, the effect of CaN on basal mitophagy is not secondary to
270 membrane potential alteration because we did not record any significant difference in
271 mitochondrial membrane potential upon expression of constitutive active CaN (Supplementary
272 figure 10).

273 Because PINK1 favours Drp1 activation via PKA displacement⁵¹ and directly phosphorylates Drp1
274 to promote Drp1-dependent fission⁵³, it is possible that in PINK1 KO MEFs, mitochondria simply do
275 not fragment to allow efficient mitochondrial autophagy. To address this hypothesis, we
276 investigated by confocal live imaging mitochondrial length of WT and PINK1 KO cells transiently
277 expressing constitutive active CaN (Δ CnA) and subjected to 3hrs CCCP. Expression of constitutive
278 active CaN promotes mitochondrial fragmentation in WT cells, which was not exacerbated in
279 presence of CCCP. On the contrary, the mitochondrial network of PINK1 KO cells did not fragment
280 when constitutive active CaN was expressed (Figure 8H-I). In addition, although PINK1 KO cells did
281 not seem to have more elongated mitochondria than WT cells under basal condition,
282 mitochondria did not fragment when treated with CCCP, indicating impaired fission in this
283 condition (Figure 8H-I).

284 Thus, in PINK1 KO MEFs expressing constitutive active CaN, mitochondria do not fragment and
285 cannot be efficiently eliminated by mitochondrial autophagy. In this condition, Parkin appears to
286 be on ubiquitinated mitochondria, and protein levels of its targets are decreased.

287 **Constitutive active Calcineurin corrects locomotor ability and mitochondrial function of PINK1** 288 **KO flies.**

289 To evaluate the physiological relevance of our finding *in vivo*, we turned to a well-established
290 *drosophila* model of mitochondrial dysfunction that was successfully used in many studies before:
291 the PINK1 KO flies⁸⁵⁻⁹². At the systemic level, PINK1 KO flies show characteristic locomotor defects

292 in flight and climbing ability, degeneration of muscle fibers of the thorax and reduced lifespan. The
293 phenotype of PINK1 KO flies can be rescued by overexpression of Parkin, whereas Parkin KO
294 phenotype, which phenocopies PINK1 KO, cannot be rescued by PINK1 overexpression, and
295 combined mutation of PINK1 and Parkin genes does not exacerbate the phenotype⁸⁶⁻⁸⁸. These
296 evidences have been interpreted as PINK1 and Parkin interacting functionally in a linear pathway
297 with PINK1 operating upstream of Parkin⁸⁶⁻⁸⁸. With that in mind and to assess the role of CaN in
298 this pathway, we evaluated the effect of CaN inhibition and activation *in vivo* in PINK1 KO flies. To
299 do so, we used a locomotor assay in which 10 flies for each strain were collected in a vertical
300 plastic tube positioned with a line drawn at 6 cm from the bottom of the tube and under a light
301 source. After tapping the flies to the bottom of the tube, the flies that successfully climbed above
302 the mark after 10 seconds were counted (Figure 9A). As already reported^{87,88}, PINK1 KO flies
303 (PINK1B9) performed poorly in the climbing assay compared to wild type (Figure 9B), and Parkin
304 overexpression (Parkin OE) rescued PINK1 KO climbing defects (Figure 9B). Feeding PINK1 KO flies
305 with CaN specific inhibitor FK506 diminished the rescuing effect of Parkin overexpression on
306 climbing performance (Figure 9C), while FK506 administration alone did not show any adverse
307 effects on the climbing ability of PINK1 KO flies (Figure 9D). Importantly, expression of CaN
308 constitutive active (CaN-A14F)⁷² in PINK1 KO background rescued PINK1 KO climbing defects
309 (Figure 9D), an effect that was suppressed by feeding flies with CaN inhibition FK506 (Figure 9D).
310 Moreover, expression of constitutive active CaN enhanced basal mitophagy in WT and PINK1 KO
311 flies (Figure 9E-F), and rescued PINK1 KO mitochondrial respiratory defects (Figure 9G-H).

312 **Discussion**

313 Mitophagy, a selective kind of autophagy during which defective mitochondria are recognized and
314 degraded, depends on Serine/threonine kinase PINK1 and E3 ubiquitin ligase Parkin⁹³, two genes
315 which mutations have been linked to the onset of an autosomal recessive juvenile
316 parkinsonism^{9,94}. Previous studies independently showed that during stress-induced mitophagy,
317 the E3 ubiquitin ligase Parkin translocates in a PINK1-dependent manner to depolarized
318 mitochondria^{33,38,46}. In this process, kinase PINK1 phosphorylates Ubiquitin⁴³, Parkin⁹⁵ and its
319 targets^{49,96}, and promotes mitochondrial Parkin translocation³⁸ and Parkin activity^{43,97}. On
320 depolarized mitochondria, Parkin ubiquitinates mitochondrial pro-fusion proteins Mitofusin
321 (Mfn)^{38,47,48,98,99} leading to its chaperone p97/VCP-mediated retrotranslocation for proteosomal
322 degradation⁴⁷. In addition, Parkin ubiquitinates the mitochondrial protein translocase TOM20,
323 mitochondrial VDAC/Porin and Fis1⁴⁸, and it also promotes the degradation of Miro⁹⁶, a protein
324 that couples mitochondria to microtubules. Selected mitochondria are therefore deprived of their
325 pro-fusion protein Mfn, they are isolated from the mitochondrial network, and driven to
326 autophagic degradation via autophagy adaptors like p62 (SQSTM1)¹⁰⁰, HDAC6¹⁰¹, Optineurin and
327 NDP52¹⁰². As shown in many studies, CCCP treatment is one of the most consolidated stimuli to
328 promote Parkin translocation and stress-induced mitophagy. CCCP triggers mitochondrial
329 depolarization by transporting protons inside the mitochondrial matrix, and induces a transient
330 increase of cytosolic Ca²⁺ influx⁵⁷ that leads to CaN activation⁵²; CaN activation promotes Drp1
331 translocation to mitochondria to induce mitochondrial fission⁵², and the transcription of
332 autophagy and lysosomal genes via TFEB⁶⁰. In perfect agreement with this coordinated set of
333 events, we found that activated CaN interacts with the mitophagic protein Parkin, and promotes
334 Parkin mitochondrial recruitment. Importantly, the effect of CaN activation on mitochondrial
335 recruitment of Parkin is PINK1-independent, and does not affect mitochondrial membrane
336 potential. Parkin-dependent mitophagy has been described in the absence of mitochondrial
337 membrane potential depolarization, following proteotoxic stress^{55,103} or upon specific induction of
338 mitochondrial Ca²⁺ oscillation¹⁰⁴. In this scenario, PINK1 is presumably not stabilized on the outer
339 mitochondrial membrane to promote Parkin recruitment because it is imported by a functional
340 mitochondrial import machinery, and rapidly degraded³⁹. Also, PINK1-independent mechanisms of
341 Parkin recruitment have been previously described¹⁰⁵. These studies suggest that Parkin
342 recruitment and Parkin-dependent mitophagy can be activated upon stimuli, which do not
343 necessarily culminate in mitochondrial damage or mitochondrial ROS production, and more

344 importantly that alternative PINK1-independent mechanisms of Parkin recruitment and activation
345 can be predicted. It is possible that additional kinases other than PINK1 can phosphorylate Parkin,
346 Ubiquitin, and prime mitochondria for Parkin recruitment and mitophagy. Parkin is a heavily
347 phosphorylated protein, and several kinases have been reported to phosphorylate Parkin (for
348 example AMPKA1¹⁰⁶, CDK5¹⁰⁷, PLK1¹⁰⁸, ULK1¹⁰⁹ and GSK3 β ¹¹⁰). It is possible that one of these
349 kinases or another kinase yet to be identified are responsible for Ubiquitin phosphorylation,
350 mitochondrial priming, and Parkin activation and recruitment, or that phospho-ubiquitin
351 independent mechanisms of Parkin activation, such as Parkin neddylation^{110,111}, are triggered by
352 CaN activation. Undoubtedly, the mechanism underlying activation and mitochondrial
353 recruitment of Parkin is not completely unravelled, and remains fertile ground for further debate.
354 Interestingly, although Parkin is efficiently recruited to mitochondria in PINK1 KO cells expressing
355 constitutive active CaN, this is not sufficient to promote mitophagy *in vitro*, presumably because in
356 MEFs, Drp1-dependent mitochondrial fission is required to allow efficient engulfment of damaged
357 mitochondria. As shown in many *in vitro* studies, the autophagic engulfment of mitochondria need
358 to be paralleled by a tight control of mitochondrial size, and mitochondria need to fragment prior
359 to mitophagy⁵⁹. Because PINK1 inhibits PKA-mediated phospho-inhibition of Drp1⁵¹ and it directly
360 phosphorylates Drp1 on S616 to regulate mitochondrial dynamic⁵³, PINK1 expression is required in
361 MEFs to release Drp1 inhibition and promote its mitochondrial recruitment to initiate
362 mitochondrial fragmentation. Following mitochondria damage, PINK1 becomes active, disrupts the
363 AKAP1-PKA and phosphorylates Drp1 to promote Drp1-dependent fission⁵¹, which is required to
364 execute mitophagy. Thus in MEFs, expression of CaN does not promote mitophagy in the absence
365 of PINK1, although Parkin is efficiently recruited to mitochondria, and protein levels of its
366 mitochondrial targets TOM20, VDAC and Mfn1 are decreased.
367 At the systemic level, CaN activation in PINK1 KO flies rescues the characteristic locomotor defects
368 in climbing ability and mitochondrial dysfunction of these flies. Importantly, in the brain of the fly
369 larvae, CaN expression enhances basal mitophagy even in the absence of PINK1 expression. This
370 result highlights a fundamental difference between CaN-dependent mitophagy in MEFs and
371 neuronal cells of the fly head: in MEFs, PINK1 expression seems to be an absolute prerequisite for
372 mitophagy execution, presumably because PINK1 is required to promote Drp1-dependent fission.
373 It is possible that in the neurons of the PINK1 KO fly brain, mitophagic events predominately occur
374 in a piece meal fashion, by selective targeting portions of mitochondria for turnover via
375 mitochondria derived vesicles (MDV)^{112,113}, a process that does not seem to require Drp1-

376 dependent fission¹¹². How mitochondrial autophagy is differentially executed in specific cell type
377 and in the complexity of the whole organism remains poorly understood, and open to new
378 discoveries.

379 As observed by others before us⁹¹, we did not see defective mitophagy in the brain of PINK1 KO
380 flies, raising questions regarding the physiological relevance of PINK1 activation *in vivo* during
381 mitophagy. One possible explanation for this lack of effect might be that PINK1-independent
382 mitophagic pathways are activated during development to compensate for PINK1 loss. Recent
383 publications provide hints toward this hypothesis, and suggest that the mitochondrial quality
384 control pathways are intertwined so that activation of one specific pathway can compensate for
385 loss of another^{84,114,115}. Nevertheless, PINK1 KO flies do present a very obvious mitochondrial
386 phenotype: mitochondrial ultrastructure is deranged, Complex I activity is compromised, and
387 mitochondrial respiration is defective^{85-87,90,116}. These conditions increase the risk of oxidative
388 stress and inflammation deriving from cytosolic release of mitochondrial DAMPs and exposure of
389 mitochondrial antigens¹¹⁷. In this scenario, enhancement of PINK1-independent mitophagy can
390 promote elimination of dysfunctional mitochondria, prevent ROS builds up, and mitigate
391 inflammation. While we cannot exclude the possibility that CaN promotes pro-survival and
392 neuroprotective pathways via functions that are independent of Parkin-driven mitophagy, our *in*
393 *vivo* results fully support the hypothesis that the rescue depends at least in part on an
394 amelioration of mitochondrial quality control, which in the fly head it occurs in the absence of
395 PINK1.

396 In conclusion, this study highlights an unprecedented role for Ca²⁺-dependent phosphatase CaN in
397 the regulation of Parkin translocation and mitophagy. A transient increase of cytosolic Ca²⁺ influx
398 promotes activation of CaN, which interacts with Parkin and induces Parkin mitochondrial
399 recruitment. In parallel, CaN activates the transcription of autophagy and lysosomal genes via
400 TFEB⁶⁰, and allows Drp1 mitochondrial recruitment and mitochondrial fission to execute
401 mitophagy (Figure 10).

402 **Materials and Methods**

403 **Cells**

404 Mouse embryonic fibroblast cells (MEFs) and Human embryonic kidney 293T (HEK293T) were
405 cultured in Dulbecco's modified Eagle medium (DMEM) (Thermo Fisher Scientific) supplemented
406 with 10% Fetal Bovine Serum (FBS), 2 mM L-glutamine, 1% MEM non-essential amino acids
407 solution, 50 U/ml penicillin and 50 µg/ml streptomycin (Thermo Fisher Scientific), and incubated at
408 37°C, in a humidified 5% CO₂ atmosphere. PINK1 wildtype and knock-out cells were kindly
409 provided by Prof. Francesco Cecconi lab (Danish Cancer Society, Denmark) and Prof. Juan Pedro
410 Bolaños lab (Universidad de Salamanca, Spain).

411 Transfection was performed using Transfectin™ Lipid Reagent (BIO-RAD) following manufacturer
412 instruction. 4-6 hours after transfection the medium was changed and cells were processed for the
413 indicated experiment 24/48 hours after. This protocol has been used both for confocal microscope
414 analysis and for protein assays. Alternatively, cells were transiently transfected with plasmid DNA
415 using PEI (Polysciences, 24765) according to manufacturer's instructions. Cells were silenced with
416 Calcineurin siRNA oligo duplex (OriGene, SR416619) by direct transfection, using Transfectin (BIO-
417 RAD) according to the protocol of the manufacturer. siRNA transfected cells were collected after
418 48hrs.

419 The following drugs were used: CCCP 10 µM (Sigma-Aldrich), Rotenone 2µM (Sigma-Aldrich),
420 Oligomycin 1 mg/ml (Sigma-Aldrich), Antimycin A 2.5 µM (Sigma-Aldrich), FK506 0.6µM (Sigma-
421 Aldrich).

422 **Constructs and Molecular Biology**

423 mCherry-Parkin and HA-Ubiquitin plasmids were obtained from Addgene. Site directed
424 mutagenesis, using QuickChange II XL kit (Agilent) and the following primers were used to
425 generate a point mutation on Serine 65 in Parkin (S65E): F-MutpkSer65E (5'- GAC CTG GAT CAG
426 CAG GCC ATT GTT CAC ATT GT- 3') and R-MutpkSer65E (5'-ACA ATG TGA ACA ATG GCC TGC TGA
427 TCC AGG TC- 3'). The same protocol was used for Ubiquitin point mutation at Serine65, and the
428 following primers were used: F-MutUbSer65E (5'-ATC CAG AAG GAG GAG ACC CTG CAC CT- 3') and
429 R-MutUbSer65E (5'- AGG TGC AGG GTC TCC TCC TTC TGG AT- 3'). These constructs were named
430 Parkin S65E and Ub-S65E.

431 Flag-tagged Parkin was inserted into pMSCV vector by using the pCR®8/GW/TOPO® TA Cloning®
432 Kit (Thermo Fisher Scientific). To perform the pCR®8/GW/TOPO® cloning, Flag-Parkin construct
433 was PCR amplified from pEYFP-C1-Parkin vector (available in the lab) using the following primers:

434 Parkin-forward-BgIII-Flag (5' -AGCT AGATCT ATG GAT TAC AAG GAT GAC GAC GAT AAG ATG ATA
435 GTG TTT GTC AGG- 3') and EYFP-reverse (5' -ACC ATG GTG AGC AAG GGC GAG- 3').

436 pcDNA3.1- Δ CnA^{H151Q} (Δ CnA^{H151Q}), pDCR-HA- Δ CnA (Δ CnA), pDCR-CnB, Drp1-YFP and variants, , and
437 mito-YFP were plasmids already available in the lab and described in^{52,118,119}. pLVX-Puro-
438 mitoKeima was kindly provided by Prof. Finkel (Center for Molecular Medicine, National Heart
439 Lung and Blood Institute, NIH Bethesda, USA).

440 GFP-LAMP1 and GFP-Rab5 were purchased from Addgene.

441 **Production of lentiviral particles and infection.**

442 pLVX-Puro-mitoKeima was kindly provided by Toren Finkel (Center for Molecular Medicine,
443 National Heart, Lung, and Blood Institute, NIH, Bethesda, MD, USA). HEK293T cells were seeded
444 onto 100 mm-diameter tissue culture Petri dishes. 24 h after plating, cells were cotransfected
445 using PEI with LV-mitokeima and the packaging plasmids pMDLg/pRRE, pRSV-Rev, pMD2.G. After 8
446 h, the transfection medium was replaced with fresh culture medium. 2 million MEFs were seeded
447 onto 60 mm Petri dishes. After 48 h, the cells medium was collected and mixed with 6 μ g/ml of
448 Polybrene (Sigma-Aldrich). Receiver MEFs were infected for 36 h, before changing the medium. All
449 procedures for the production and use of lentiviral particles were performed in a biosafety level-2
450 (P2) environment.

451 **Retroviral infection and generation of Parkin-flag stable cell lines.**

452 To generate Parkin-flag retroviruses, HEK 293T cells were plated at 2 M cells/100-mm-diameter
453 tissue culture dishes and transfected with the pN8E VSGV, Gag-pol packaging vectors and the
454 retroviral vector (empty or containing Parkin-flag) by PEI (Polyscience) direct transfection. At 5 h
455 post-transfection, the medium was replaced with fresh DMEM containing 10% FBS, and cells were
456 grown for an additional 24 h, before the transfection was repeated. After 24 h, the conditioned
457 medium containing recombinant retroviruses was collected and filtered through 0.45 μ m-pore-
458 size filters. Samples of these supernatants were applied immediately to MEFs cells, which had
459 been plated 18 h before infection at a density of 10⁵ cells/60-mm-diameter tissue culture dishes.
460 Polybrene (Polyscience) was added to a final concentration of 6 μ g/ml, and the supernatants were
461 incubated with the cells for 24 h. After infection, the cells were placed in fresh growth medium
462 and cultured in DMEM culture medium. Selection with 200 μ g of Hygromycin B/ml (Sigma-Aldrich)
463 was initiated 24 h after infection. After about 15 days, cells were expanded.

464 **Immunofluorescence (IF)**

465 For Ubiquitin-TOM20 immunostaining, MEFs transiently expressing constitutively active CaN or
466 corresponding empty vector were pretreated with 50 μ M proteasome inhibitor Mg132 (Sigma-
467 Aldrich) for 30 min. Cells were then fixed with 4% PFA in PBS for 15 min at room temperature,
468 permeabilized with 0,1% Triton X-100 in PBS, and blocked with BSA 4% in PBS supplemented with
469 0,05% Tween20. Cells were incubated overnight with the following antibodies: Ubiquitin (1:100;
470 Enzo Life Science; BML-PW8810) and TOM20 (1:200; Santa Cruz; sc-11415). Cells were washed
471 three times in PBS supplemented with 0,05% Tween20 and subsequently incubated with the
472 corresponding Alexa secondary antibodies (Thermo Fisher Scientific).

473 **Imaging**

474 For confocal imaging experiments of Parkin localization, transfected MEFs cells were seeded onto
475 24 mm-round glass coverslips in 6-well culture plates. Cells were co-transfected with mCherry-
476 Parkin construct together with mito-YFP. When indicated, cells where cotransfected with CnB, the
477 regulatory Calcineurin (Cn) domain, plus Δ CnA (constitutively active Cn) or Δ CnAH151Q (dominant
478 negative mutant of Cn), and/or one of the Ubiquitin constructs (Ub or UbS65E). Image analysis was
479 performed using ImageJ. These constructs were then excited using 561nm or 488nm laser and
480 using a *UPlanSApo 60x/1.35* objective (iMIC Andromeda). Stack of images separated by 0.2 μ m
481 along the z-axis were acquired. The quantification was performed as calculation of the percentage
482 of cells with Parkin puncta on mitochondria or through an ImageJ plugin for colocalization
483 quantification (see following paragraph for details).

484 **Image analysis using Squassh**

485 To quantify Parkin colocalization with mitochondria, we created maximum-intensity projections of
486 z-series with 0.2 μ m increments. Quantification was then performed by using 'Squassh'
487 (Segmentation and QUAntification of Subcellular SHapes), a plugin compatible with the imaging
488 processing softwares ImageJ or Fiji, freely available from [http://mosaic.mpi-](http://mosaic.mpi-cbg.de/?q=downloads/imagej)
489 [cbg.de/?q=downloads/imagej](http://mosaic.mpi-cbg.de/?q=downloads/imagej). Squassh is a segmentation method that enables both colocalization
490 and shape analyses of subcellular structures in fluorescence microscopy images⁶². For Parkin-
491 mitochondria colocalization analysis, segmentation was performed with the minimum intensity
492 threshold for the first channel set to 0.35, for the second to 0.15 and the regularization weight to
493 0.015. Among the three different colocalization coefficients (C_{signal} , C_{number} and C_{size}), we
494 preferentially used C_{number} . It has to be noted that Squassh based analysis is unbiased as this
495 method is completely automated and performed by computer software.

496 Colocalization analysis of Ubiquitin with TOM20 was performed on single plane images using
497 Squassh. For this analysis, segmentation was performed with the minimum intensity threshold for
498 the first channel set to 0.2, for the second to 0.2 and the regularization weight to 0.05. As
499 colocalization coefficient we used C_{number} .

500 **Mitokeima mitophagy analysis by flow cytometry.**

501 Mitokeima expressing MEFs were analyzed by flow cytometry (BD FACSAria™ sorter) as previously
502 reported¹²⁰. Cells were analyzed with flow cytometer equipped with a 405-nm and a 561-nm laser.
503 Cells were excited with violet laser (405 nm) with emission detected at 610±10nm with a BV605
504 detector and with a yellow-green laser (561 nm) with emission detected at 610±10nm by a PE-
505 CF594 detector simultaneously.

506 **Immunoblotting**

507 At the established time points, the medium was removed and MEFs washed with ice-cold PBS.
508 After withdrawing PBS, cells were scraped off the wells using a plastic cell scraper, they were
509 resuspended in 1,5 ml of cold PBS and they were centrifuged at 3'000g at 4 °C for 5 min.
510 Supernatant was discarded and then the pellet was resuspended in an appropriate volume of
511 radioimmunoprecipitation assay (RIPA) buffer (150 mM NaCl, 50 mM Tris-HCl, 1% NP-40, 0.25%
512 Sodium Deoxycholate, 1 mM EDTA in distilled water and adjusted pH to 7.4) with freshly added
513 protease inhibitors cocktail (PIC). Cells were kept on ice for 30 min. Lysate were cleared by
514 centrifugation at 20'000 g for 15 min at 4 °C.

515 Protein concentrations of samples was determined using Pierce™ BCA Protein Assay Kit (Thermo
516 Fisher scientific).

517 NuPAGE® LDS Sample Buffer (Invitrogen) and 2-Mercaptoethanol (Sigma-Aldrich) were mixed to
518 samples and proteins were then denaturated at 95°C for 15 min. Proteins were separated on
519 ExpressPlus™ PAGE gels (GenScript) and transferred to PVDF membrane (MERCK-Millipore).
520 Membranes were incubated with indicated antibodies and imaged with ImageQuant LAS4000.
521 Band densitometry quantification was performed using ImageJ software. The following antibodies
522 were used: Actin (1:5000; Chemicon; MAB1501), ATP5A (1:5000; Abcam; ab14748), Calcineurin
523 (1:1000; BD Bioscience; 556350 and 1:1000; Abcam; ab52761), His (1: 5000; Proteintech; 66005-1),
524 Mfn1 (1:600; Proteintech; 13798-1-AP) Parkin (1:1000, Santa Cruz; SC32282), Parkin (1:500,
525 Abclonal; A0968), FLAG (1:3000; Cell Signalling; 2368S), TOM20 (1:2000; Santa Cruz; sc-11415),
526 VDAC (1:1000; Abcam; ab15895) . Canonical secondary antibodies used were sheep anti-mouse or

527 donkey anti-rabbit HRP (GE Healthcare). Mouse TrueBlot® ULTRA: Anti-Mouse Ig HRP (Rockland)
528 was used for immunoprecipitation experiment.

529 **Thermal Stability Assay**

530 Cells were plated onto 100 mm Petri dishes (10 M/dish). After 24hrs, transfection was performed
531 using PEI (Polyscience) with Δ CnA and CnB plasmids and the corresponding empty vectors. After
532 48 h from the transfection, cells were resuspended in PBS and snap-frozen in liquid nitrogen. The
533 solution was aliquot into a PCR strip and incubated at the indicated temperatures for 3 min. The
534 lysates were centrifuged at 16'000 g for 30 min at 4 °C. The soluble fraction was loaded into SDS-
535 PAGE gel.

536 **In vitro interaction assay**

537 Bacterial expression Parkin construct (NM_004562.2 GI:169790968) was transformed into BL21
538 DE3 E. Coli. Overnight culture inoculated from fresh colony was grown in Terrific broth media
539 containing 2% glucose and 50 μ g/ml kanamycin at 37°C. The following morning overnight
540 cultures were diluted to OD 600 0.1 and continued shaking at 37°C until OD 600 reached 0.8,
541 flasks were transferred to 4 °C, cultures were then induced with 0.2mM IPTG and expression was
542 allowed to proceed overnight at 18°C. Cells were harvested by centrifugation at 6'000 g for 15
543 min at 4 °C. For purification of Parkin construct, bacteria were resuspended in buffer A (50mM
544 Hepes pH 8.0, 200mM NaCl, 10mM imidazole, 250 μ M TCEP and EDTA-free Complete protease
545 inhibitor tablets (Roche)) and lysed using a French Press homogenizer. The lysate was cleared at
546 45'000g for 25min at 4°C and the supernatant was loaded into HisPur NiNTA Chromatography
547 1 ml cartridge (Thermo Fisher Scientific). The resin was washed with 50 ml of buffer A containing
548 20mM imidazole. IMAC purification was performed on an ÄKTA Purifier FPLC system (GE
549 Healthcare) and 20 fractions were eluted in imidazole gradient (20 mM ÷ 500 mM) for 20 min.
550 After elution, the protein was desalted using Vivaspin™ ultrafiltration spin columns into Buffer A
551 without imidazole. The protein was then loaded onto a HiLoad Superdex 75 16/60 size exclusion
552 chromatography column (GE Healthcare) that had been pre-equilibrated in Hepes 30 mM, NaCl
553 150 mM, Glycerol 10%. Collected fractions were then concentrated and loaded on Buffer A
554 equilibrated NeutrAvidin agarose resin (Thermo Fisher) for 40 min at 4 °C. In parallel, CaN-flag
555 expressing cells were lysed and protein extract was incubated with Parkin-bound resin overnight
556 at 4 °C under gentle rotation. The resin was washed three times and boiled at 95 °C in 2X Laemmli
557 buffer (160 mM Tris-HCl, pH 6.8, 4% SDS, 0.7 M Sucrose, 4% β -mercaptoethanol) in order to elute
558 the protein sample and subsequently resolved it in a SDS-PAGE. As negative control for the assay

559 we used USP14-Flag, a protein that is not supposed to interact with Parkin. USP14-Flag expressing
560 cells were lysed and protein extract was incubated with Parkin-bound resin and processed as just
561 described. As additional negative control, we immobilized MEF2D-His¹²¹, a protein that is not
562 supposed to interact with Calcineurin. CaN-Flag expressing cells were lysed and protein extract
563 was divided in two fractions: first fraction was incubated with Parkin-bound resin, while the
564 second fraction with MEF2D-bound resin overnight. Samples were processed as previously
565 described.

566 **Proximity Ligation Assay (PLA)**

567 For proximity ligation assay, we used a PLA kit from Sigma-Aldrich (Sigma-Aldrich DUO92014), and
568 followed the manufacturer's instructions. HeLa cells were grown on coverslips and transiently
569 transfected with mCherry Parkin and PPP3CB-Flag using Trans-IT transfection reagent (Mirus Bio)
570 for 18 h. They were then fixed with 4% paraformaldehyde (Electron Microscopy Sciences, Hatfield,
571 Pennsylvania) for 10 min at room temperature. The blocking buffer (0.5% bovine serum albumin,
572 0.1% saponin, 50 mM NH₄Cl in PBS) was then added to the cells for 20 min. The samples were
573 washed in PBS and incubated overnight at 4°C with the primary antibodies in the blocking buffer.
574 The following antibodies were used for the PLA experiments: anti-GM130 (1:700; BD Biosciences);
575 anti-PPP3CB (Origene, 1:200); anti-GRASP65 (1:1000) and anti-Parkin (1:1000) were from Abcam;
576 Alexa 488-, Alexa 633- and Alexa 568-conjugated secondary antibodies (1:400) were from
577 Invitrogen. As negative controls we used anti GRASP65, which is not supposed to interact with
578 Parkin. As positive controls, we performed the PLA by using GRASP65 and GM130. The PLA was
579 performed according to the manufacturer instructions. Finally, Hoechst was incubated for 10 min
580 at room temperature. The coverslips were then mounted on glass microscope slides with
581 Mowiol4-88 (Sigma-Aldrich). Immunofluorescence samples were examined using a confocal laser
582 microscope (Zeiss LSM700 confocal microscope system; Carl Zeiss, Gottingen, Germany) equipped
583 with ×63 1.4 NA oil objective. Optical confocal sections were taken at 1 Airy unit, with a resolution
584 of 512 × 512 pixels or 1.024 × 1024 pixels. PLA analysis was performed using Fiji. Images were
585 subjected to thresholding, and the number of particles ("PLA dots") was calculated with the
586 Analyze Particles function. As negative controls we used anti GRASP65, which is not supposed to
587 interact with Parkin. As positive control, we performed the PLA by using GRASP65 and GM130
588 (both expressed in the cis golgi network⁷⁴).

589 **Co-Immunoprecipitation assay**

590 MEFs and HEK293T cells were pretreated with 10 μM CCCP for 2 h and cell pellet was resuspended

591 in ice-cold lysis buffer (Hepes 50 mM, Tween-20 0,1%, Triton X-100 1%, Glycerol 10% with freshly
592 added phosphatase and protease inhibitor, pH 7.2). Cells were kept on ice for 30 min and the
593 soluble fractions from cell lysates were isolated by centrifugation at 12,000g for 15 min. In the
594 meantime, 50 μ l of Protein-A Agarose (Roche) were washed and equilibrated in lysis buffer.
595 Protein extract was pre-cleared in the equilibrated resin with 30 min incubation at 4 °C. Pre-
596 cleared sample was quantified using Pierce™ BCA Protein Assay Kit (Thermo Fisher Scientific). For
597 co-immunoprecipitations, 5 mg of lysate was incubated with Parkin antibody (2 μ g; Santa Cruz
598 32282) or with Calcineurin antibody (2 μ g; BD Bioscience 556350). Anti-mouse IgG was used in
599 both cases as negative control (2 μ g; Santa Cruz sc-2025) with constant rotation overnight at 4 °C.
600 Then, 50 μ l of Protein-A beads (Roche) was added to lysates and incubated with rotation for 2 h at
601 4 °C. After incubation, the resin was washed three times in ice-cold PBS and the samples were
602 eluted in Laemmli buffer with β -mercaptoethanol at 70 °C for 15 min and loaded on 8% SDS-PAGE.

603 **Electron microscopy**

604 Samples were fixed with 2.5% glutaraldehyde in 0.1M sodium cacodylate buffer pH 7.4 ON at 4°C.
605 The samples was postfixed with 1% osmium tetroxide plus potassium ferrocyanide 1% in 0.1M
606 sodium cacodylate buffer for 1 hour at 4°. After three water washes, samples were dehydrated in
607 a graded ethanol series and embedded in an epoxy resin (Sigma-Aldrich). Ultrathin sections (60-
608 70nm) were obtained with an Ultratome V (LKB) ultramicrotome, counterstained with uranyl
609 acetate and lead citrate and viewed with a Tecnai G2 (FEI) transmission electron microscope
610 operating at 100 kV. Images were captured with a Veleta (Olympus Soft Imaging System) digital
611 camera.

612 **Mitochondria membrane potential analysis**

613 Mitochondria membrane potential was measured with the fluorescent dye Tetramethylrhodamine
614 Methyl Ester (TMRM). MEFs cells were previously seeded on 24 mm round coverslips and
615 transfected with Δ CnA + CnB plasmids or with the corresponding empty vectors. 48 hours after
616 transfection, cells were washed with HBSS containing 20mM HEPES (pH 7.4). Cells were then
617 incubated in HBSS with 1 μ M Cyclosporin H and 10nM TMRM for 30 min at 37°C. Cellular
618 fluorescence images were acquired at room temperature with UPlanSApo 60x/1.35 objective (iMIC
619 Andromeda). Sequential images were acquired every 1 min. After 5 min, 2.5 μ g/ml Oligomycin was
620 added directly into the acquisition chamber. After 30 min, mitochondria were fully depolarized by
621 the addition of 2 μ M of the protonophore carbonylcyanide-p-trifluoromethoxyphenyl hydrazone
622 (FCCP) and recorded for further 5min. Images were analyzed using Image J software. Mitochondria

623 network of each cell was identified as region of interest (ROI) and field not containing cells was
624 used as background. The mean fluorescence intensity was measured for each ROI. Following
625 background subtraction, each value of TMRM fluorescence was normalized with initial
626 fluorescence and expressed as relative TMRM intensity.

627 **Fly stocks and breeding conditions**

628 Flies were raised on standard cornmeal medium and were maintained at 23° C, 70% relative
629 humidity, on a 12 h light : 12 h dark cycle.

630 We used ActGal4 or nSybGal4 standard lines crossed with w1118, generous gifts from Dr.
631 Alexander Whitworth (University of Sheffield) as controls. PINK1B9 and PK OE lines were already
632 described before^{86,87} and were a kind gift from Dr. Alexander Whitworth. Mito-QC line was also a
633 kind gift from Dr. Alexander Whitworth⁹¹. CanA-14F line was described before¹²² and was a kind
634 gift by Dr Pascal Dijkers.

635 **Climbing assay**

636 The climbing assay (negative geotaxis assay) was used to assess locomotor ability. Climbing data
637 were obtained from groups of untreated wildtype, untreated PINK1B9, FK506-treated wildtype,
638 and FK506-treated PINK1B9. Briefly, 10 flies for each strain were collected in a vertically-
639 positioned plastic tube (length 12 cm; diameter 5 cm) with a line drawn at 6 cm from the bottom
640 of the tube. Flies were gently tapped to the bottom of the tube, and the number of flies that
641 successfully climbed above the 6-cm mark after 10 seconds was noted. Fifteen separate and
642 consecutive trials were performed for each experiment, and the results were averaged. At least 30
643 flies were tested for each genotype or condition.

644 The number of flies that could climb unto, or above, this line within 10 or 20 seconds was recorded
645 and expressed as percentage of total flies.

646 **Analysis of mitochondrial respiration in flies**

647 The rate of mitochondrial O₂ consumption was monitored using an Oxytherm System (Hansatech)
648 with magnetic stirring and temperature control, maintained at 30°C. Five adult male flies per
649 genotype were homogenized in respiration buffer (120 mM sucrose, 50 mM KCl, 20 mM Tris-HCl, 4
650 mM KH₂PO₄, 2 mM MgCl₂, 1 mM EGTA, 1 g/l fatty acid-free BSA, pH 7.2) and the following
651 additions were made: proline 10 mM, glutamate 10 mM, malate 4 mM, ADP 2.5 mM, oligomycin 2
652 μM, CCCP 1.25 μM, antimycin 1.25 μM. O₂ consumption was obtained from the registered slope of
653 the graph. Respiratory control ratio (RCR), state III versus state IV (ADP-stimulated respiration over

654 oligomycin-administered respiration), was also determined from the registered graphs. Data from
655 10–11 independent experiments were averaged.

656 **Analysis of mitophagy in flies (Mito-QC analysis)**

657 Brains from third instar larvae were dissected in PBS and fixed in 4% formaldehyde, pH 7, for 20
658 minutes, rinsed in PBS and mounted in Prolong Diamond Antifade mounting medium (Thermo
659 Fischer Scientific). Samples were generally dissected in the morning and imaged in the afternoon
660 of the same day. Because X chromosome nondisjunction is present in multiple balanced PINK1B9
661 mutant stocks, correct genotypes were determined by PCR-based genotyping of discarded tissue
662 after dissection.

663 Fluorescence imaging was conducted using a confocal microscope (Andromeda iMIC spinning disc
664 live cell microscope, TILL Photonics, 60× objective). Z-stacks were acquired at 0.2 μm-steps.

665 Confocal images were analyzed using Fiji (ImageJ) software. The mito-QC Counter plugin was used
666 to quantify the number of mitolysosomes, according to Montava-Garriga et al¹²³.

667 **Statistical analysis**

668 We used Origin 7.0 Professional or Prism 8 for statistical analysis. All data are expressed as mean ±
669 SEM unless specified otherwise. Statistical significance was measured by an unpaired t-test or one-
670 way or two-way ANOVA followed by *ad hoc* multiple comparison test. p-values are indicated in the
671 figure legend. Data information: n=number of biological replicate; *P ≤ 0.05, **P ≤ 0.01, ***P ≤
672 0.001, ****P ≤ 0.0001.

673 **Funding**

674 This work was supported by grants from Italian Ministry of Health “Ricerca Finalizzata” [GR-2011-
675 02351151], Rita Levi Montalcini “Brain Gain” program and Michael J. Fox RRIA 2014 [Grant ID
676 9795] to E.Z.

677 **Acknowledgements**

678 We thank Dr Alexander Whitworth for kindly providing fly lines described in Materials and
679 methods. We thank PF Dijkers for the CanA-14F fly line and F Cecconi who provided PINK1 wild
680 type and KO MEFs.

681 **Conflict of interests**

682 Authors declare no conflict of interests

683 **Data availability**

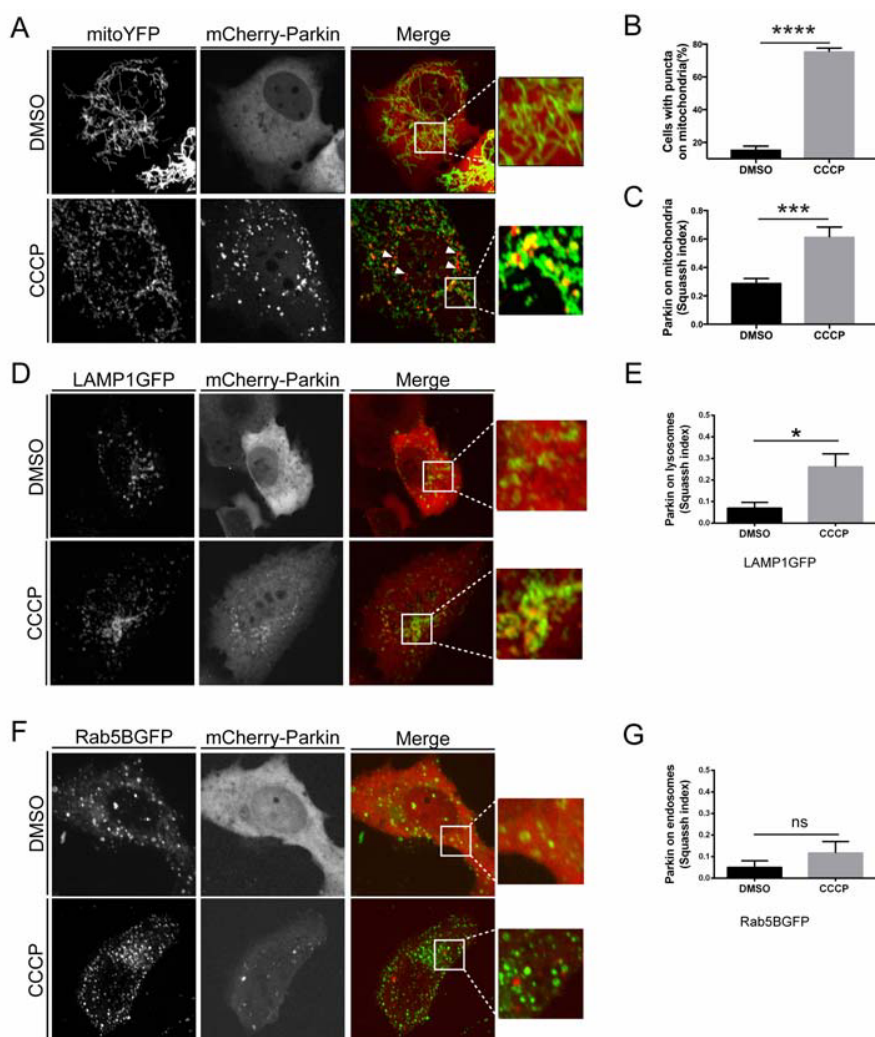
684 We confirm that all relevant data are available from the authors

685

686

687 **Figures**

688



689

690

691 **Figure 1: Parkin translocation to mitochondria is regulated by Calcineurin**

692 (A) Representative confocal images of MEF cells transfected with mCherry-Parkin and mito-YFP for
693 2 days before being treated with DMSO or 10 μ M CCCP for 3 hours. The panels on the right show
694 enlarged merged views of the boxed areas

695 (B) Quantification of A. Graph bar shows mean \pm SEM of percentage of cells with mCherry-Parkin on
696 mitochondria for at least ≥ 300 cells per biological replicate. Student's t-test (n=9-10; p<0.0001).

697 (C) Quantification of A by using Squassh. The graph bars show mean \pm SEM of Squassh
698 colocalization coefficient for at least ≥ 50 images per biological replicate. 0=no colocalization,
699 1=perfect colocalization. Student's t-test (n=5; p<0.0001)

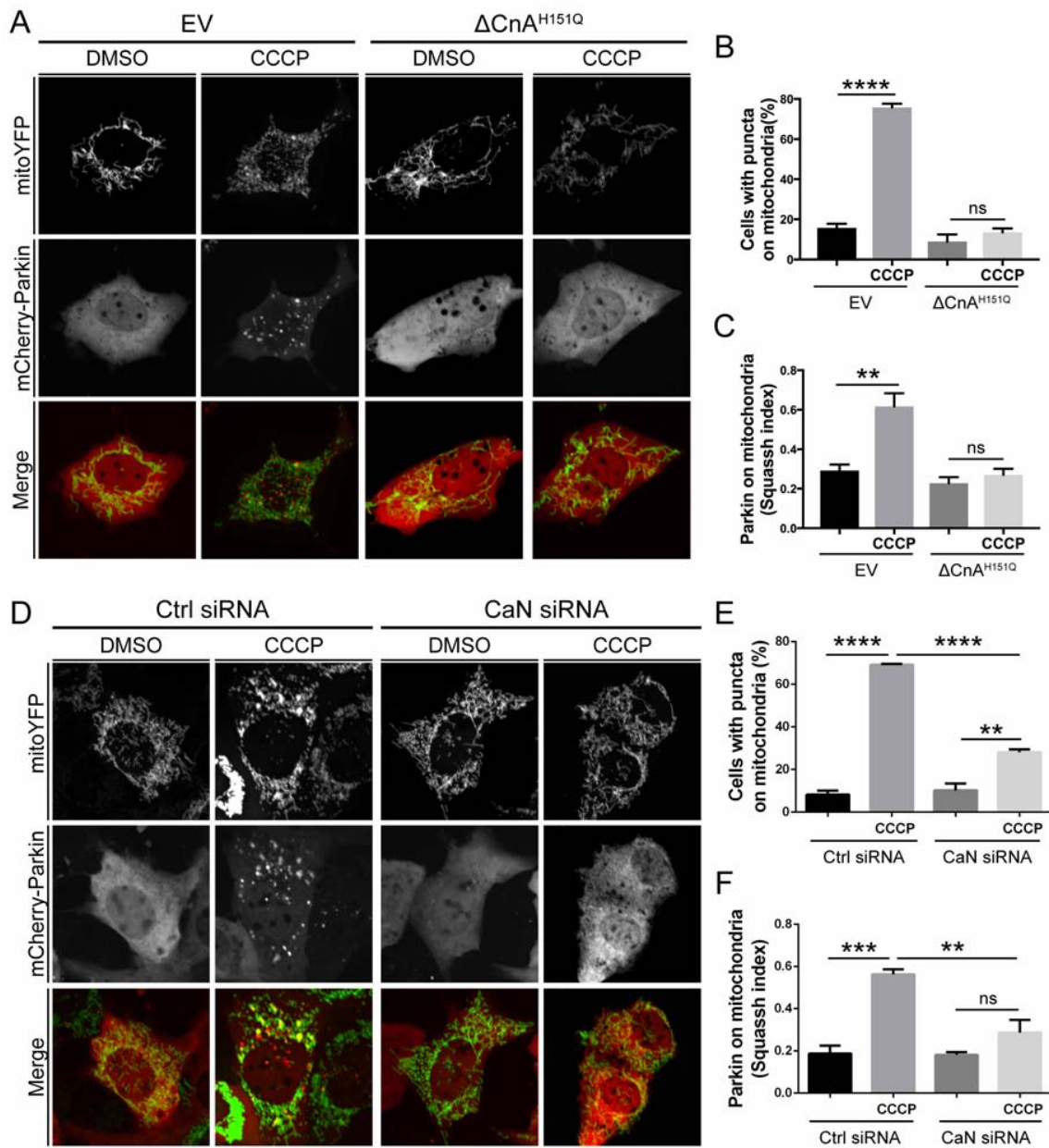
700 (D) Representative confocal images of MEF cells transfected with mCherry-Parkin and LAMP1GFP
701 for 2 days and treated with 10 μ M CCCP for 3 hours.

702 (E) Quantification of D by using Squassh. The graph bars show mean \pm SEM of Squassh
703 colocalization coefficient for at least ≥ 50 images per biological replicate. Student's t-test (n=3;
704 p<0.05)

705 (F) Representative confocal images of MEF cells transfected with mCherry-Parkin and with
706 Rab5GFP for 2 days and treated with 10 μ M CCCP for 3 hours

707 (G) Quantification of F by using Squassh. The graph bars show mean \pm SEM of Squassh
708 colocalization coefficient for at least ≥ 50 images per biological replicate. Student's t-test (n=3;
709 p<0.05).

710



711

712

713 **Figure 2: Parkin translocation to mitochondria is regulated by Calcineurin**

714 (A) Representative confocal images of MEF cells transfected with mCherry-Parkin, mito-YFP and
715 dominant negative CaN ($\Delta\text{CnA}^{\text{H151Q}}$) or the empty vector (EV) for 2 days before being treated with
716 DMSO or 10 μM CCCP for 3 hours.

717 (B) Quantification of (A). Graph bar shows mean \pm SEM of percentage of cells with mCherry-Parkin
718 on mitochondria for at least ≥ 300 cells per biological replicate. Two-way ANOVA followed by
719 Tukey's multiple comparison test ($n=3-9$; $p<0.0001$).

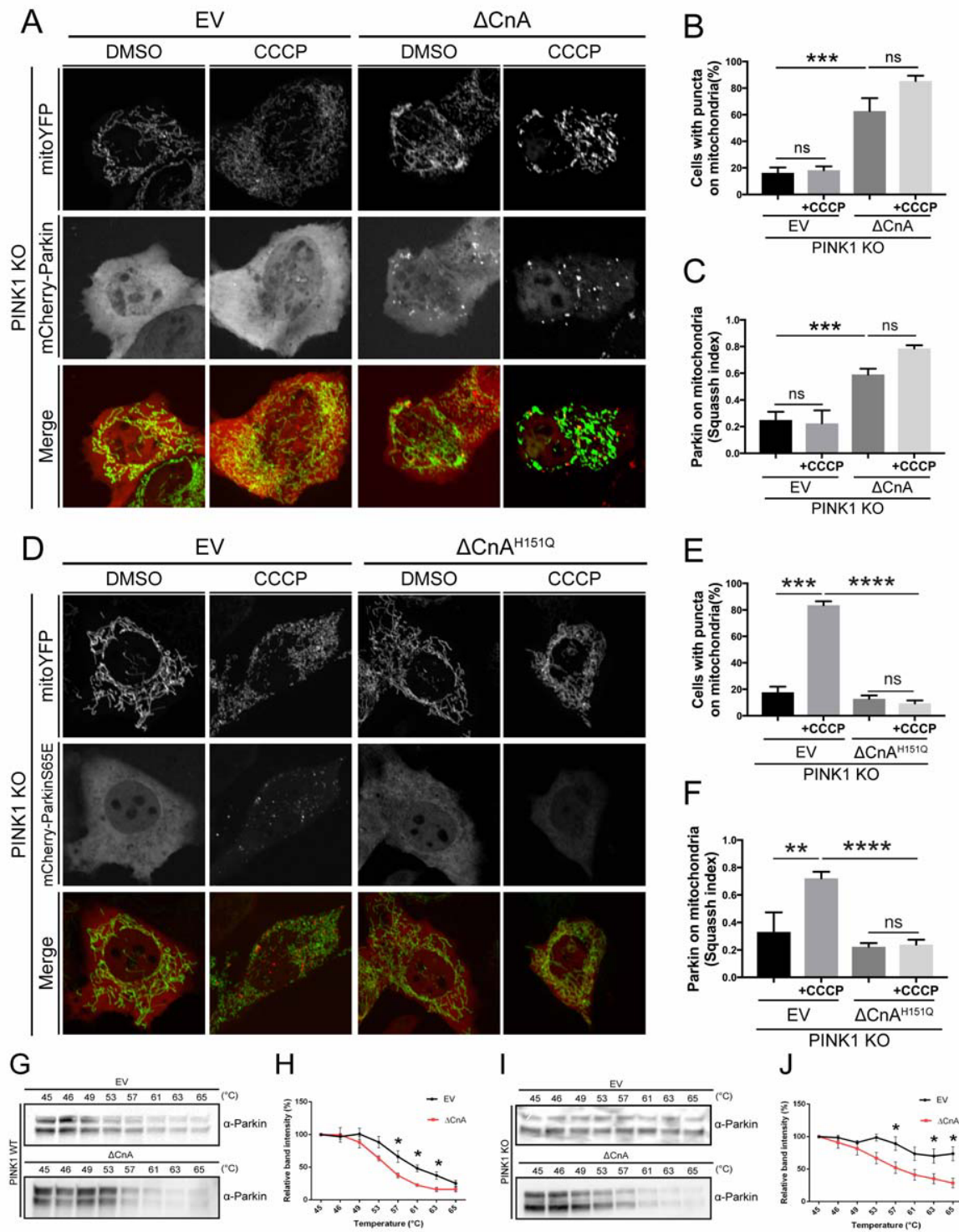
720 (C) Quantification of (A) using Squassh. The graph bars show mean \pm SEM of Squassh colocalization
721 coefficient for at least ≥ 50 images per biological replicate. 0=no colocalization, 1=perfect
722 colocalization. Two-way ANOVA followed by Tukey's multiple comparison test ($n=4-5$; $p<0.001$)

723 (D) Representative confocal images of MEF cells transfected with mCherry-Parkin, mito-YFP in
724 which CaN was downregulated, and relative control.

725 (E) Quantification of (D). Graph bar shows mean \pm SEM of percentage of cells with mCherry-Parkin
726 on mitochondria for at least ≥ 300 cells per biological replicate. Two-way ANOVA followed by
727 Tukey's multiple comparison test ($n=3$; $p<0.01$).

728 (F) Quantification of (D) using Squassh. The graph bar shows mean \pm SEM of Squassh colocalization
729 coefficient for at least ≥ 50 images per biological replicate. 0=no colocalization, 1=perfect
730 colocalization. At least 3 independent experiments were performed. Two-way ANOVA followed by
731 Tukey's multiple comparison test ($n=3$; $p<0.01$)

732



733

734

735 **Figure 3: Parkin translocation is induced by Calcineurin in the absence of PINK1**

736 (A) Representative confocal images of PINK1 KO MEF cells transfected with mCherry-Parkin, mito-
737 YFP and with empty vector (EV) or constitutively active CaN (Δ CnA).

738 (B) Quantification of (A) Graph bar shows mean \pm SEM of percentage of cells with mCherry-
739 Parkin on mitochondria for at least ≥ 300 cells per biological replicate. Two-way ANOVA followed
740 by Tukey's multiple comparison test (n=3-4; p<0.001).

741 (C) Quantification of (A) using Squassh. The graph bars show mean \pm SEM of Squassh colocalization
742 coefficient for at least ≥ 50 images per biological replicate. 0=no colocalization, 1=perfect
743 colocalization. At least 3 independent experiments were performed. Two-way ANOVA followed by
744 Tukey's multiple comparison test (n=3-4; p<0.001).

745 (D) Representative confocal images of PINK1 KO MEF cells transfected with mCherry-ParkinS65E,
746 UbS65E, mito-YFP and with empty vector (EV) or dominant negative CaN (Δ CnA^{H151Q})

747 (E) Quantification of (D) Graph bar shows mean \pm SEM of percentage of cells with mCherry-Parkin
748 on mitochondria for at least ≥ 300 cells per biological replicate. Two-way ANOVA followed by
749 Tukey's multiple comparison test (n=4; p<0.0001).

750 (F) Quantification of (D) using Squassh. The graph bars show mean \pm SEM of Squassh colocalization
751 coefficient for at least ≥ 50 images per biological replicate. 0=no colocalization, 1=perfect
752 colocalization. Two-way ANOVA followed by Tukey's multiple comparison test (n=4; p<0.0001).

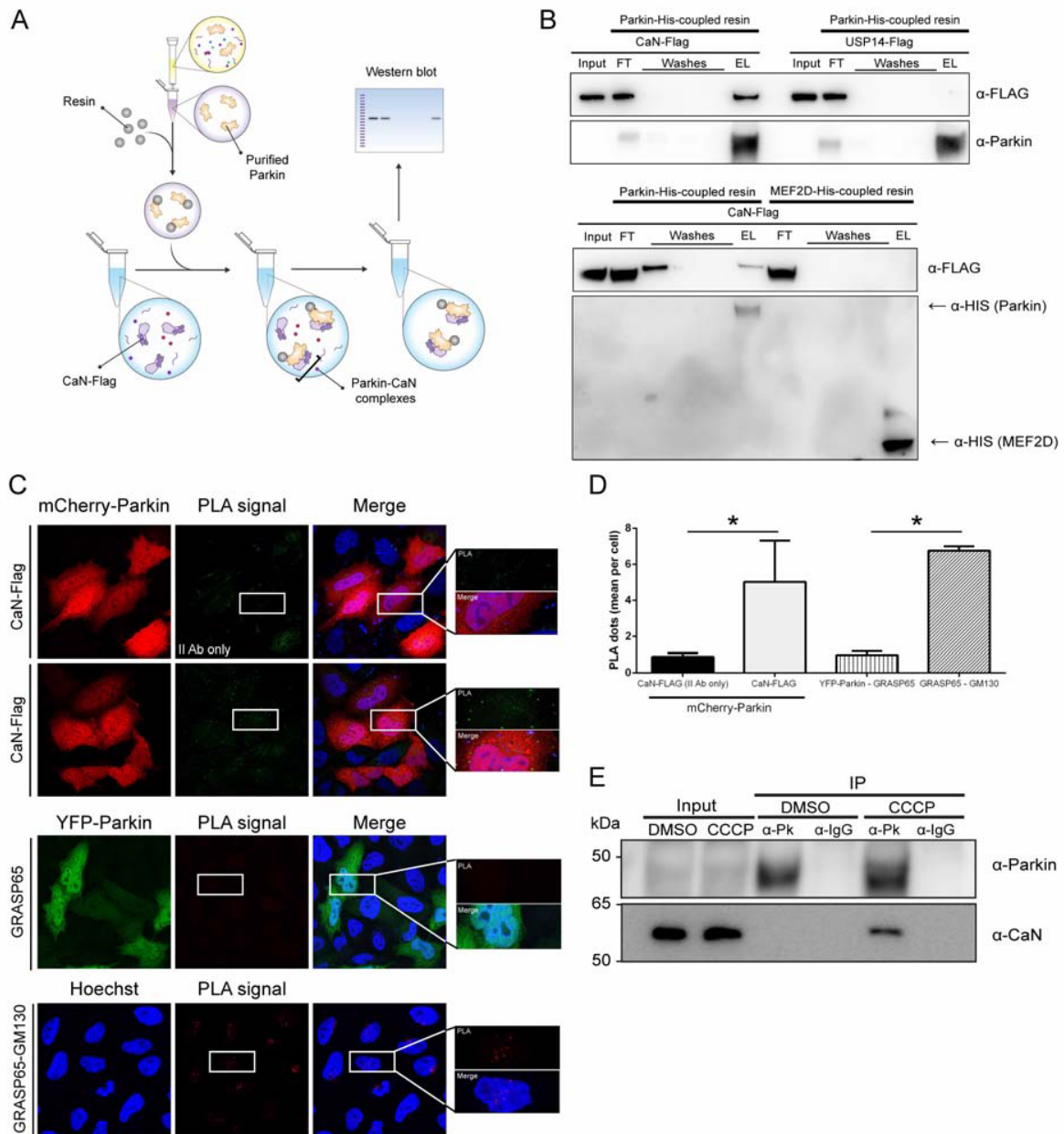
753 (G) Parkin thermal stability assay. WT MEFs expressing constitutive active CaN (Δ CnA) or empty
754 vector (EV) were suspended in PBS and snap-frozen in liquid nitrogen before being aliquoted into
755 a PCR strip and incubated at the indicated temperature for 3 min. The lysates were centrifugated
756 at high speed and the soluble fraction was loaded into SDS-PAGE gel. Representative Western
757 blotting analysis for Parkin stability is shown.

758 (H) Densitometric analysis of (G). Student's t-test (n=4; p<0.05).

759 (I) Parkin thermal stability assay. PINK1 KO MEFs expressing constitutive active CaN (Δ CnA) or
760 empty vector (EV) were suspended in PBS and snap-frozen in liquid nitrogen before being
761 aliquoted into a PCR strip and incubated at the indicated temperature for 3 min. The lysates were
762 centrifugated at high speed and the soluble fraction was loaded into SDS-PAGE gel. Representative
763 Western blotting analysis for Parkin stability is shown.

764 (J) Densitometric analysis of (I). Student's t-test (n=6; p<0.05).

765



766

767

768 **Figure 4: Calcineurin interacts with Parkin**

769 (A) *In vitro* interaction assay: schematic representation. Affinity-purified recombinant His-tagged
770 Parkin is produced from bacteria, and coupled to a His-affinity resin to generate Parkin-His-resin.
771 The resin is incubated with protein lysate extracted from cells expressing Flag-tagged CaN. The
772 resin is washed to remove nonspecifically adhering proteins, and Imidazole is used to elute the
773 complexes from the resin. The obtained eluate is separated by SDS-PAGE and analyzed by
774 immunoblotting.

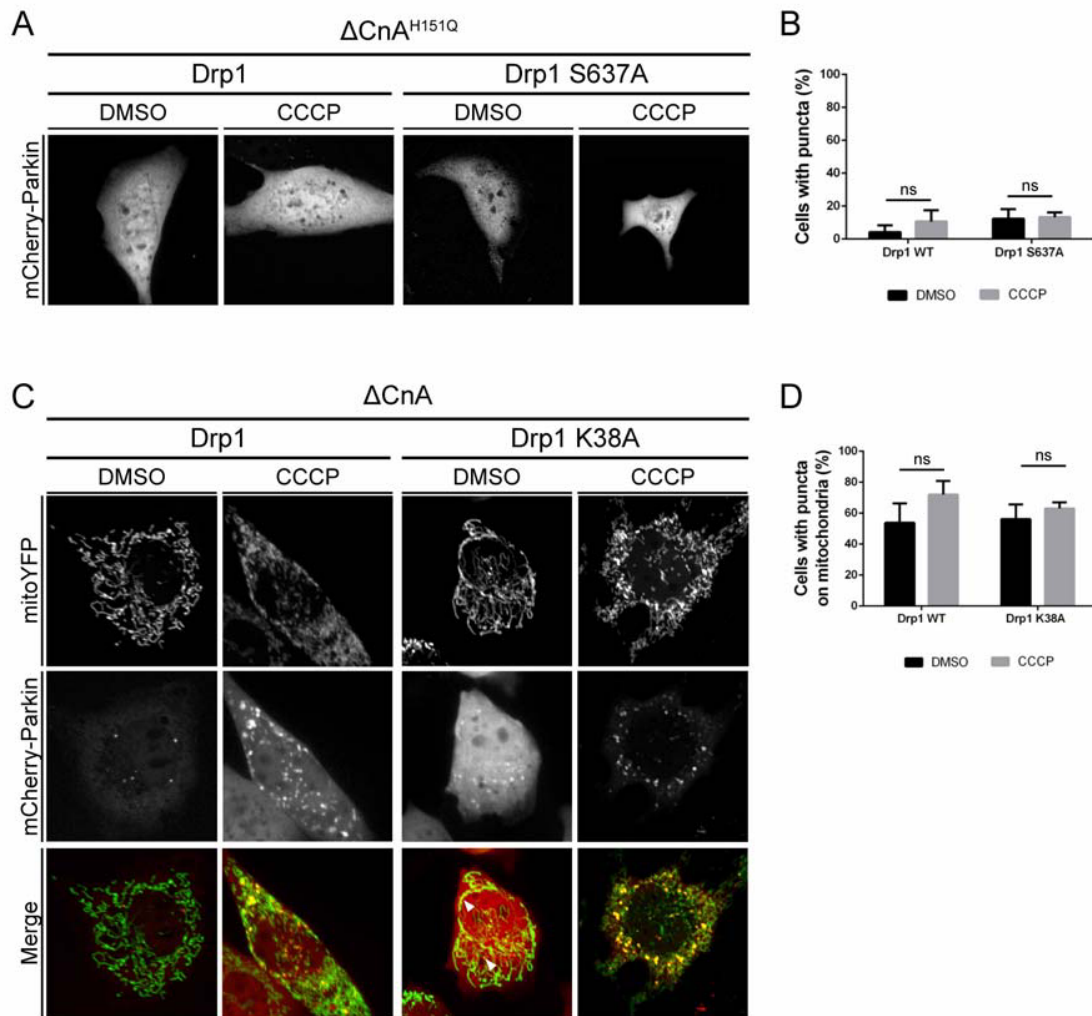
775 (B) *In vitro* interaction assay. His-tagged Parkin or His-tagged MEF2D coupled to a His-affinity resin
776 are incubated with cell lysate obtained from MEFs transfected with CaN-Flag or USP14-Flag, as
777 indicated. The eluate is separated by SDS-PAGE and analyzed by immunoblotting using anti-Flag,
778 anti-Parkin and anti-His antibodies (FT=flow through; EL=eluate).

779 (C) Representative images of Proximity Ligation Assay (PLA) performed on HeLa cells transfected
780 with Parkin-mCherry and CaN-FLAG (PPP3CB-FLAG). After fixation, cells were processed for
781 investigating Parkin proximity interactions by incubating with anti-Parkin antibody and anti-
782 PPP3CB antibody, and corresponding secondary antibodies, or secondary antibodies alone as
783 negative control. CaN and Parkin interactions are represented by green dots. As negative
784 biological control for PLA we used anti-Parkin antibody and anti-GRASP65 antibody in YPF-Parkin
785 expressing HeLa cells. As positive control for PLA, we used anti-GRASP65 antibody and anti-GM130
786 antibody. GRASP65 is a peripheral membrane protein that resides in the *cis*-Golgi apparatus, and
787 interacts with GM130 (also expressed in the *cis*-Golgi network) but not with Parkin. GRASP65 and
788 GM130 interactions are represented by red dots. White squares contain higher-magnification
789 images.

790 (D) Quantification of (C). Graph bar shows (mean \pm SEM of PLA dots per cell for at least ≥ 350 cells
791 per biological replicate. Student's t-test ($n=3-4$; $p<0.05$)

792 (E) HEK 293T cells were treated with DMSO or CCCP-2hrs and subjected to immunoprecipitation
793 (IP) of Parkin using mouse anti-Parkin antibody or anti-mouse IgG as negative control. Western
794 Blot analysis was performed with rabbit anti-CaN antibody or mouse anti-Parkin antibody on the
795 pulled down samples. Inputs represent 5% of the protein lysates and IP eluate 100% of the protein
796 lysates. Mouse IgG TrueBlot® ULTRA enabled detection of Parkin band, without hindrance by
797 interfering immunoprecipitating IgG heavy chains.

798



799

800

801 **Figure 5: Parkin translocation is induced by Calcineurin independently of Drp1 mitochondrial**
802 **recruitment and activity**

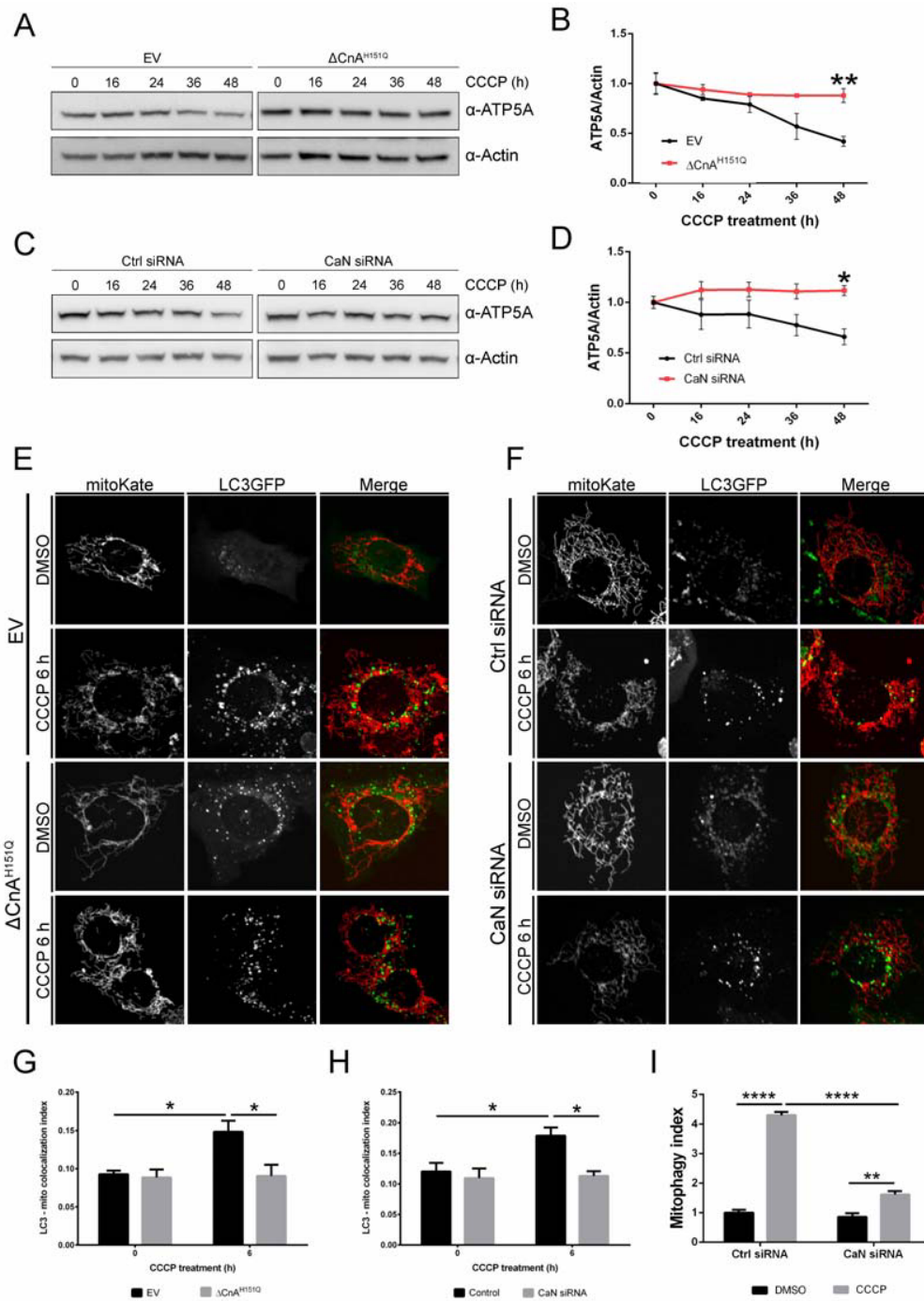
803 (A) Representative confocal images of wild type MEF cells transfected with mCherry-Parkin and
804 YFP-Drp1 or YFP-Drp1 S637A plus dominant negative CaN ($\Delta\text{CnA}^{\text{H151Q}}$) for 2 days before being
805 treated with DMSO or 10 μM CCCP for 3 hours.

806 (B) Quantification of A. Graph bar shows mean \pm SEM of percentage of cells with mCherry-Parkin
807 puncta for ≥ 300 cells per biological replicate. Two-way ANOVA followed by Tukey's multiple
808 comparison test (n=3).

809 (C) Representative confocal images of wild type MEF cells transfected with mCherry-Parkin, mito-
810 YFP and constitutive active CaN (ΔCnA) plus Drp1 or Drp1 K38A for 2 days before being treated
811 with DMSO or 10 μM CCCP for 3 hours.

812 (D) Quantification of C. Graph bar shows mean \pm SEM of percentage of cells with mCherry-Parkin
813 on mitochondria for ≥ 300 cells per biological replicate. Two-way ANOVA followed by Tukey's
814 multiple comparison test (n=3;).

815



816

817

818 **Figure 6: Calcineurin is required for CCCP-induced mitophagy**

819 (A) Western blot analysis of protein lysates extracted from MEFs expressing empty vector (EV) or
820 dominant negative CaN ($\Delta\text{CnA}^{\text{H151Q}}$). Cells were treated with 10 μM CCCP for the indicated time.

821 (B) Quantification of (A). Line chart shows mean \pm SEM of ATP5A protein level normalized to Actin.
822 Student's t-test (n=3; p<0.01).

823 (C) Western blot analysis of protein lysates extracted from MEFs downregulating Calcineurin and
824 control. Cells were treated with 10 μM CCCP for the indicated time.

825 (D) Quantification of (C). Line chart shows mean \pm SEM of ATP5A protein level normalized to Actin.
826 Student's t-test (n=5; p<0.05)

827 (E) Representative confocal images of cells transfected with LC3GFP and MitoKate plus dominant
828 negative CaN ($\Delta\text{CnA}^{\text{H151Q}}$) or empty vector (EV).

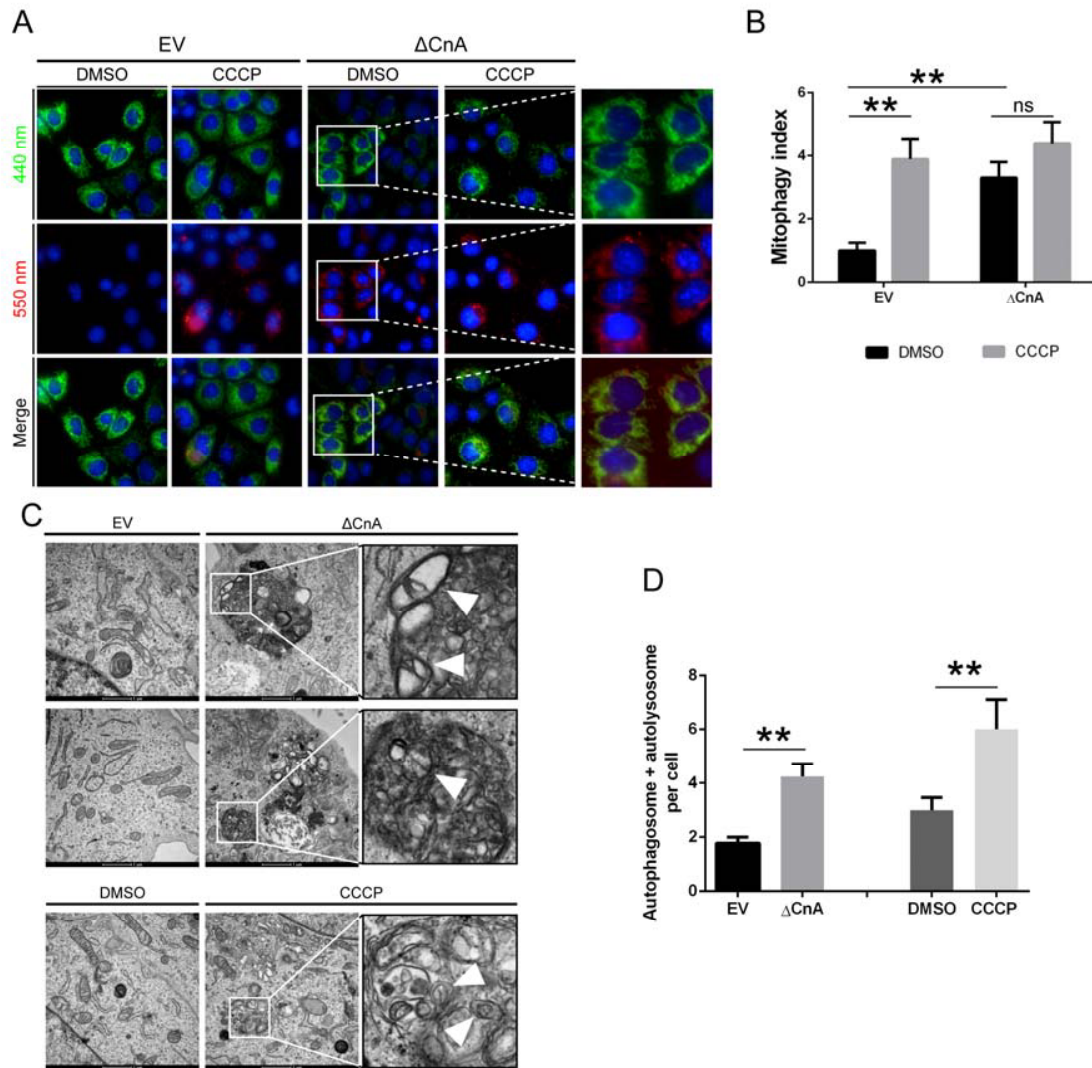
829 (F) Representative confocal images of cells transfected with LC3GFP and MitoKate in CaN
830 downregulating condition and matching control.

831 (G) Quantification of (E) using Squassh. Two-way ANOVA followed by Tukey's multiple comparison
832 test (n=3; p<0.05)

833 (H) Quantification of (F) using Squassh. Two-way ANOVA followed by Tukey's multiple comparison
834 test (n=3; p<0.05)

835 (I) mt-Keima analysis in CaN downregulation condition upon CCCP treatment. mt-Keima
836 demonstrates a greater than 4-fold change in ratiometric fluorescence in CCCP treated cells, which
837 was blunted upon CaN downregulation. Two-way ANOVA followed by Tukey's multiple
838 comparison test (n=3; p<0.001).

839



840

841

842 **Figure 7: Calcineurin is required for CCCP-induced mitophagy**

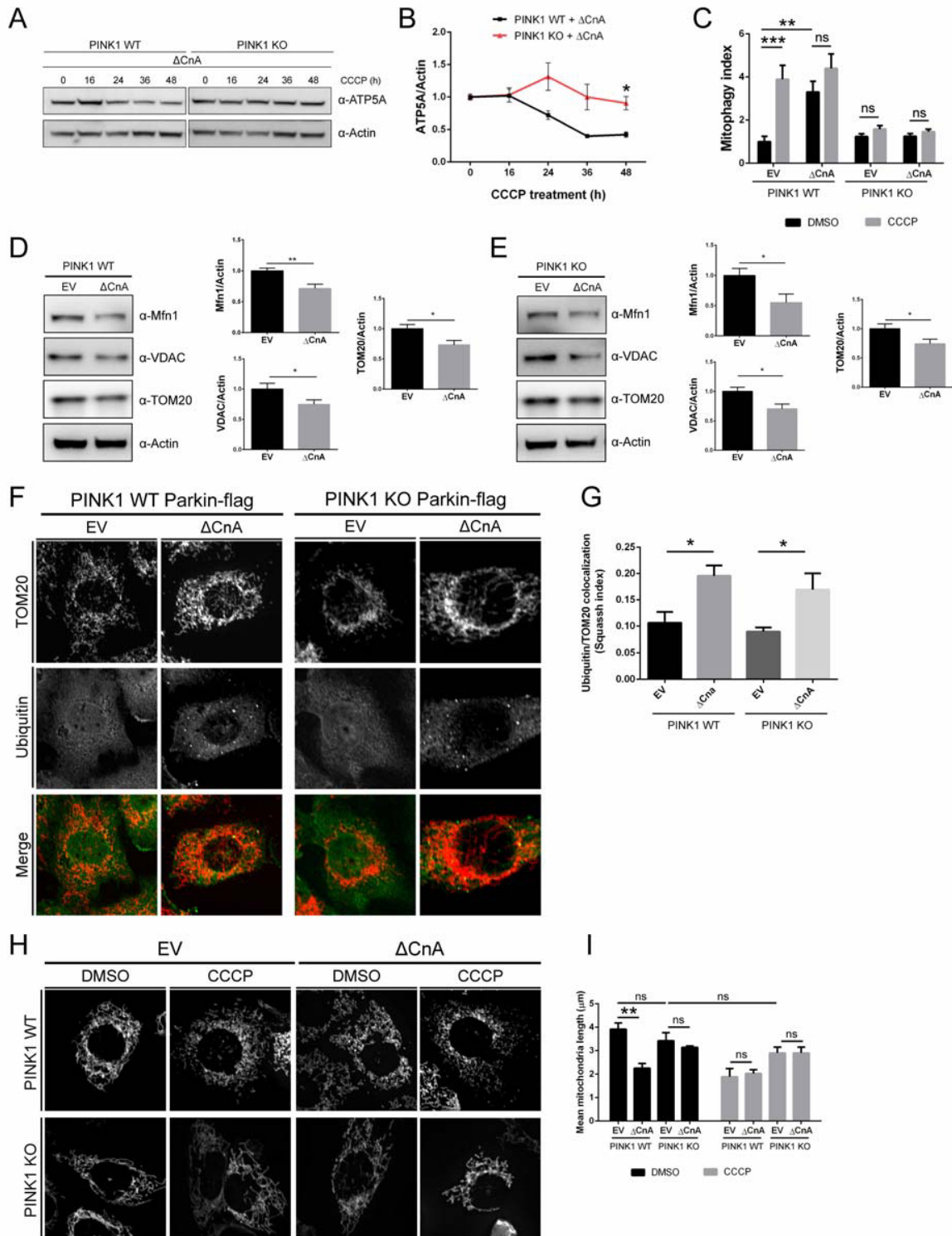
843 (A) Representative image of mt-Keima expressing cells acquired on confocal microscope Operetta
844 High-Content Imaging system. MEFs were transfected with constitutive active CaN (Δ CnA) or
845 empty vector (EV).

846 (B) mt-Keima analysis in MEFs expressing constitutive active CaN (Δ CnA) and relative control (EV).
847 Two-way ANOVA followed by Tukey's multiple comparison test (n=6; p<0.01).

848 (C) Representative electron microscope images showing the presence of autophagosomes with
849 mitochondrial-like structures inside in MEFs expressing constitutive active CaN (Δ CnA) and control
850 (EV). 24hrs CCCP-treated cells were used as positive control. Mitochondrial-like structures were
851 identified as described in Chakraborty et al.¹²⁴

852 (D) Bar graph represents mean \pm SEM of the number of autophagosomes and autolysosomes per
853 cell. At least 60 cells per biological replicate were analyzed from each group. Student's t-test (n=3-
854 4; p<0.01).

855



856

857

858 **Figure 8: Calcineurin requires PINK1 and mitochondrial fission to induce mitophagy in MEFs**

859 (A) Representative Western blot analysis of protein lysates extracted from PINK1 WT and KO
860 MEFs. Cells were transfected with constitutive active CaN (Δ CnA) and after 2 days they were
861 treated with 10 μ M CCCP for the indicated time.

862 (B) Quantification of (A). Line chart shows mean \pm SEM of ATP5A protein level normalized to Actin.
863 Student's t-test (n=5; p<0.05).

864 (C) mt-Keima analysis of wild type (WT) and PINK1 KO MEFs. Cells were transfected with
865 constitutive active CaN (Δ CnA) or empty vector (EV) for 2 days before being treated with DMSO or
866 10 μ M CCCP for 3hrs, and subjected to FACS analysis. Two-way ANOVA followed by Tukey's
867 multiple comparison test (n=6; p<0.01).

868 (D) Representative Western blot analysis of protein lysates extracted from PINK1 WT and KO
869 MEFs. Cells of the indicated genotype were transfected with constitutive active CaN (Δ CnA) or
870 empty vector (EV). Graph bars shows mean \pm SEM of indicated mitochondrial protein level
871 normalized to Actin. Student's t-test (n=8; p<0.001).

872 (E) Representative Western blot analysis of protein lysates extracted from PINK1 WT and KO MEFs.
873 Cells of the indicate genotype were transfected with constitutive active CaN (Δ CnA) or empty
874 vector (EV). Graph bars shows mean \pm SEM of indicated mitochondrial protein level normalized to
875 Actin. Student's t-test (n=11; p<0.05).

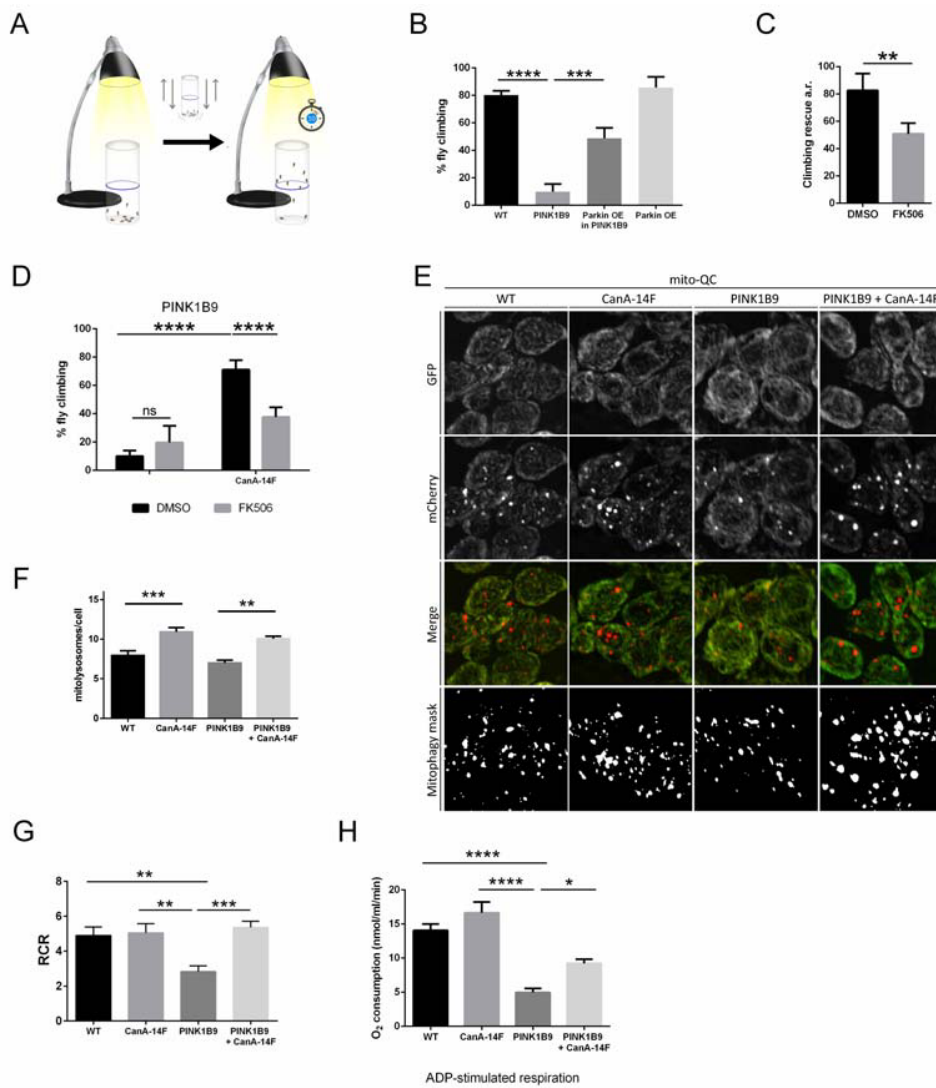
876 (F) Representative confocal images of cells of the indicated genotype transfected with constitutive
877 active CaN (Δ CnA) or empty vector (EV). Cells were pretreated with proteasome inhibitor MG132
878 before being fixed, permeabilized and incubated with the indicated primary antibodies and
879 corresponding fluorophore-conjugated secondary antibodies.

880 (G) Quantification of (F) using Squassh. Two-way ANOVA followed by Tukey's multiple comparison
881 test (n=4; p<0.05).

882 (H) Representative confocal images of cells of the indicated genotype transfected with mito-YFP
883 and constitutive active CaN (Δ CnA) or empty vector (EV), treated with DMSO or 10 μ M CCCP for
884 3hrs.

885 (I) Quantification of (H) using Squassh. The graph bar shows mean \pm SEM of mean object length of
886 each image for at least \geq 70 images per biological replicate. Two-way ANOVA followed by Tukey's
887 multiple comparison test (n=3; p<0.05).

888



889

890

891 **Figure 9: Constitutive active Calcineurin corrects locomotor ability and mitochondrial function of**
892 **PINK1 KO flies.**

893 (A) Schematic representation of the climbing assay. 10 flies were put into a tube in a dark room. A
894 light was put on the top of the tube. After tapping the flies at the bottom of the tube, the number
895 of flies that successfully climbed above the 6-cm mark after 10 seconds was recorded.

896 (B) Graph bar shows mean \pm SEM of the climbing performance of flies of the indicated genotype.
897 One-way ANOVA followed by Sidak's multiple comparison test (n=5; p \leq 0.001).

898 (C) Graph bar shows mean \pm SEM of the climbing rescue (arbitrary unit) of PINK1 KO flies (PINK1B9)
899 overexpressing Parkin and treated as indicated for 48hrs with DMSO or FK506. Student's t-test
900 (n=5; p \leq 0.01).

901 (D) Graph bar shows mean \pm SEM of the climbing performance of PINK1 KO flies (PINK1B9) upon
902 expression of constitutive active calcineurin (CanA-14F), and treated as indicated for 48hrs with
903 DMSO or FK506. Two-way ANOVA followed by Sidak's multiple comparison test (n=5; p \leq 0.001).

904 (E) Representative confocal microscopy images of neurons in the ventral nerve chord of third
905 instar larvae. Fluorescence corresponding to neutral pH (GFP) and acidic pH (mCherry) are shown.
906 Mitolysosomes are counted as GFP-negative/mCherry-positive (red-only) puncta. The mitophagy
907 mask generated by the mito-QC Counter allows visualization of the quantified mitophagy areas¹²³.

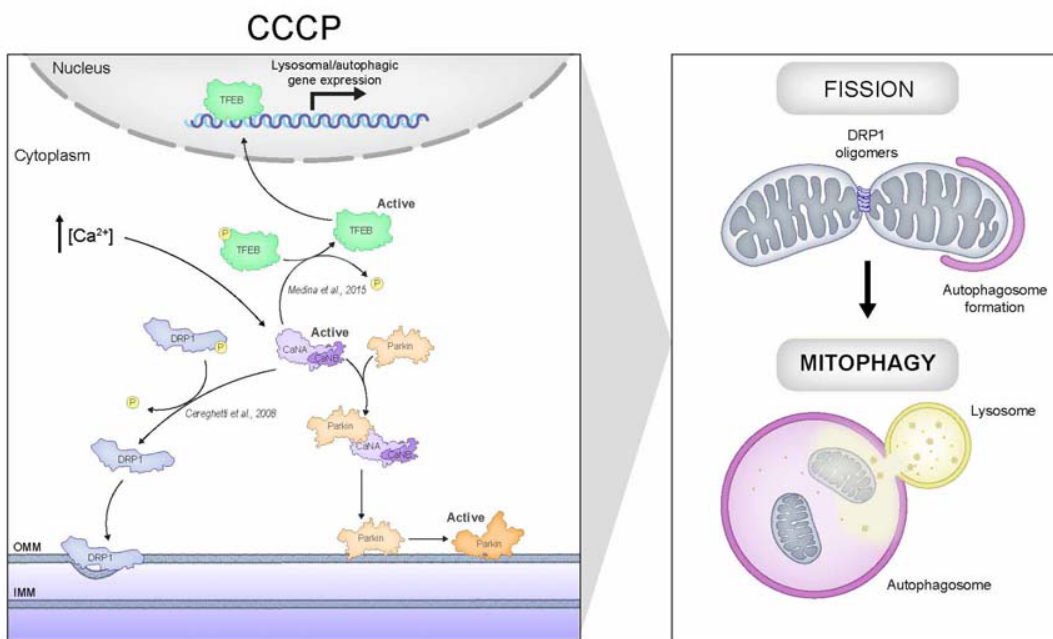
908 (F) Quantification of total number of mitolysosomes per cell using the mito-QC Counter¹²³ (Fiji). At
909 least 40 cells were analyzed per animal. One way ANOVA followed by Sidak's test for multiple
910 comparisons (n=6; p \leq 0.01).

911 (G) Quantitative analysis of respiratory fitness of mitochondria from adult flies of the indicated
912 genotype. Graph shows respiratory control ratio (RCR) calculated as described in Materials and
913 Methods. One-way ANOVA followed by Sidak's test for multiple comparison test (n=10-11, p \leq
914 0.01).

915 (H) Quantitative analysis of respiratory fitness of mitochondria from adult flies of the indicated
916 genotype. Graph bar shows ADP-stimulated respiration calculated as described in Materials and
917 Methods. One-way ANOVA followed by Sidak's test for multiple comparison test (n=10-11, p \leq
918 0.01).

919

920



921

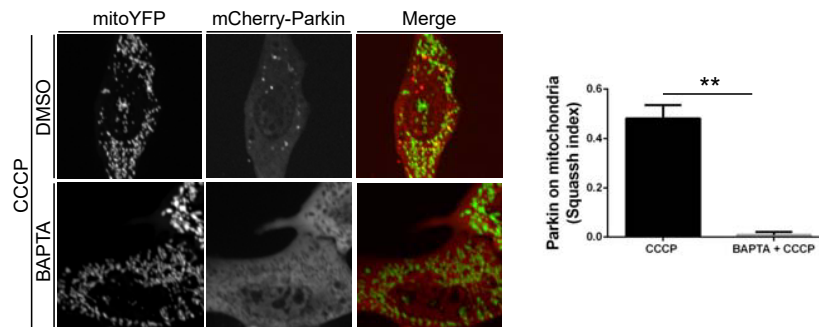
922

923 **Figure 10: Schematic representation of the pathway regulating Parkin translocation and**
924 **mitophagy induced by Calcineurin.**

925 Mitochondrial membrane potential drives PINK1 import into healthy mitochondria through the
926 TOM and TIM complexes. Once on the IMM, PINK1 gets cleaved by MPP and PARL and eventually
927 degraded by the ubiquitin-proteasome system^{46,125}. In this scenario, CaN is not active and Parkin is
928 kept in the cytosol.

929 Mitochondria depolarization induced by CCCP is followed by cytosolic Ca²⁺ rise^{57,125}, which
930 activates CaN¹²⁶. Activated CaN promotes mitochondrial recruitment of Drp1 and Drp1-dependent
931 mitochondrial fission by dephosphorylating Drp1⁵². Activated CaN also promotes
932 dephosphorylation of TFEB to induce its activation and the expression of autophagy and lysosomal
933 genes⁶⁰. In parallel, CaN interacts with Parkin and promotes Parkin translocation to mitochondria
934 in a PINK1-independent fashion. The interaction between CaN and Parkin might be direct or via a
935 binding partner.

936



937

938

Supplementary Figure 1: Parkin translocation to mitochondria is regulated by Calcineurin

939

Representative confocal images of wild type MEFs transfected with mCherry-Parkin and mito-YFP

940

for 2 days before being treated with 40 μ M BAPTA for 30 min or with 40 μ M BAPTA for 30 min

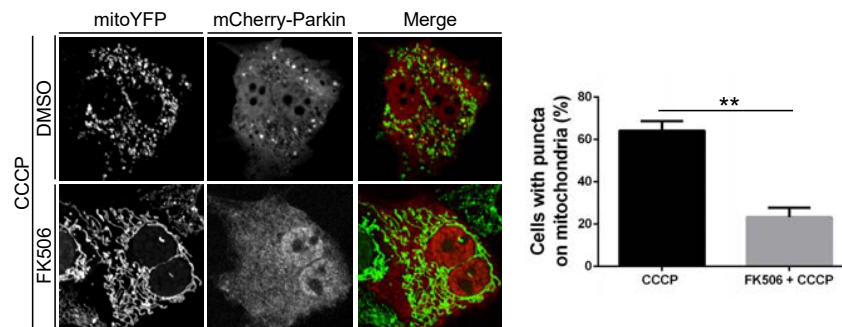
941

prior to 3 hrs 10 μ M CCCP treatment, as indicated. Graph bar shows mean \pm SEM of percentage of

942

cells with mCherry-Parkin on mitochondria. Student's test (n=3; p<0.01).

943



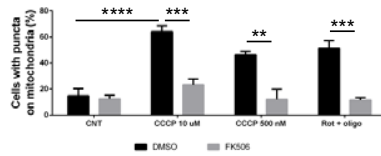
944

945 **Supplementary Figure 2: Parkin translocation to mitochondria is regulated by Calcineurin**

946 Representative confocal images of wild type MEFs transfected with mCherry-Parkin and mito-YFP
947 for 2 days before being treated with 0.6 μ M FK506 for 30 min or with 0.6 μ M FK506 for 30 min
948 prior to 3hrs/10 μ M CCCP treatment, as indicated. Graph bar shows mean \pm SEM of percentage of
949 cells with mCherry-Parkin on mitochondria for at least ≥ 300 cells per biological replicate.

950 Student's test (n=3; p<0.01).

951

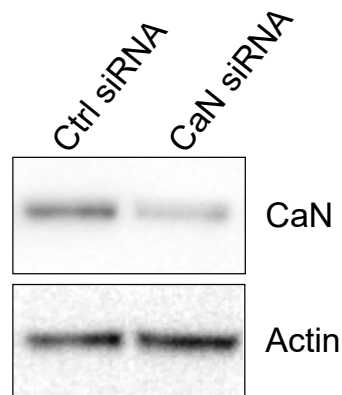


952

953 **Supplementary Figure 3: Parkin translocation to mitochondria is regulated by Calcineurin**

954 Graph bar shows mean±SEM of percentage of cells with mCherry-Parkin on mitochondria for at
955 least ≥ 300 cells per biological replicate. Cells were transfected with mCherry-Parkin and after 2
956 days they were treated as indicated. One-way ANOVA followed by Tukey's multiple comparison
957 test (n=3; p<0.01).

958

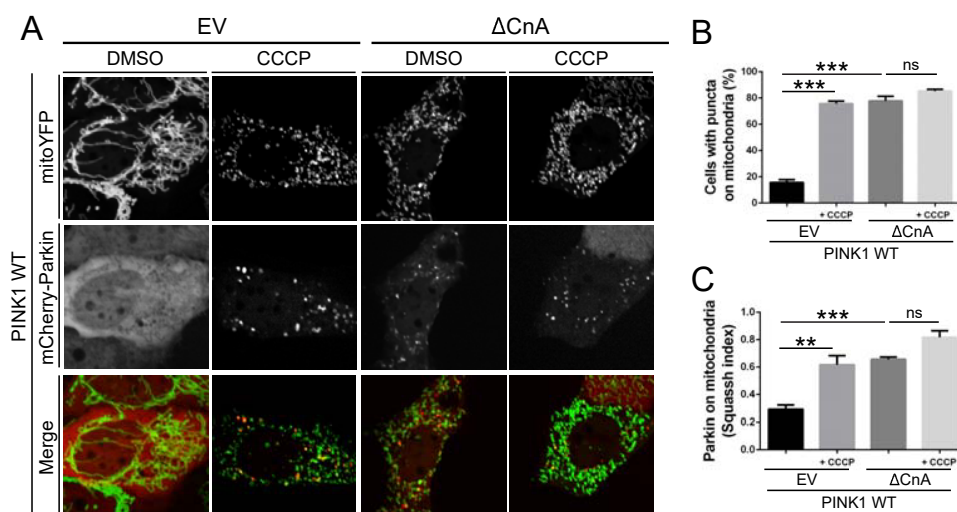


959

960 **Supplementary Figure 4: Parkin translocation to mitochondria is regulated by Calcineurin**

961 Western blot analysis of protein lysates extracted from MEFs downregulating Calcineurin and
962 relative control. Cells were treated with CaN siRNA and control siRNA, protein lysates were
963 collected after 2 days and subjected to Western blotting analysis with the indicated antibodies.

964



965

966

Supplementary Figure 5: Parkin translocation to mitochondria is regulated by Calcineurin

967

(A) Representative confocal images of wild type MEFs transfected with mCherry-Parkin, mito-YFP and with empty vector (EV) or constitutively active CaN (Δ CnA) for 2 days before being treated with DMSO as control or 10 μ M CCCP for 3hrs.

970

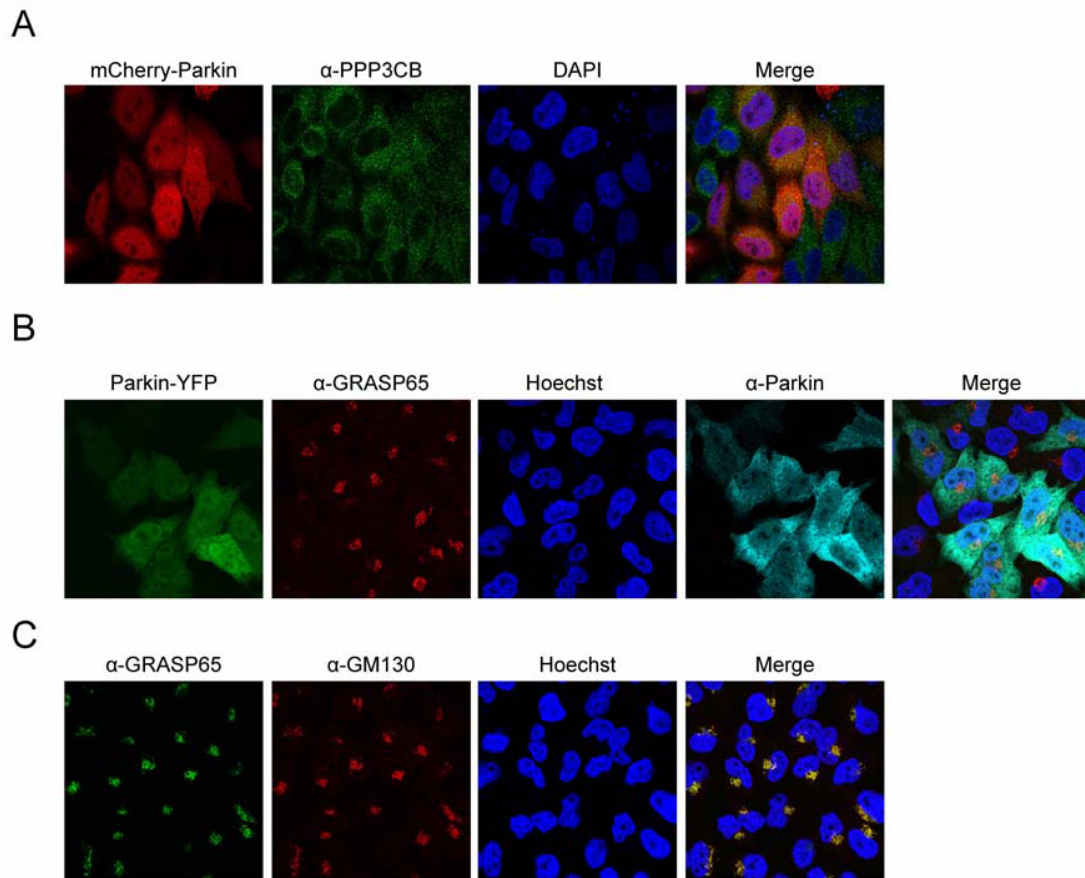
(B) Quantification of A. Graph bar shows mean \pm SEM of percentage of cells with mCherry-Parkin on mitochondria for at least \geq 300 cells per biological replicate. Two-way ANOVA followed by Tukey's multiple comparison test (n=3-9; p<0.001).

973

(C) Quantification of A by using Squassh. The graph bars show mean \pm SEM of Squassh colocalization coefficient for at least \geq 50 images per biological replicate. 0=no colocalization, 1=perfect colocalization. Two-way ANOVA followed by Tukey's multiple comparison test (n=3-4; p<0.01).

976

977



978

979 **Supplementary Figure 6: Calcineurin interacts with Parkin**

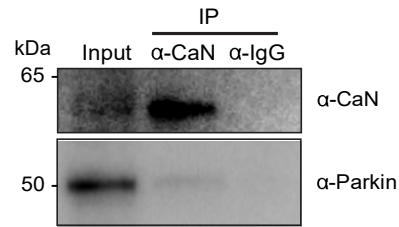
980 (A) Representative images of HeLa cells transfected with mCherry-Parkin and probed with
981 antibody against Calcineurin (PPP3CB). Cells were fixed, permeabilized and incubated with the
982 indicated primary antibody, corresponding fluorophore-conjugated secondary antibody, and DAPI
983 for nuclear staining.

984 (B) Representative images of HeLa cells transfected with Parkin-YFP probed with antibodies
985 against GRASP65 and Parkin. Cells were fixed, permeabilized and incubated with the indicated

986 primary antibodies, corresponding fluorophore-conjugated secondary antibodies, and Hoechst for
987 nuclear staining. GRASP65 is a *cis*-Golgi resident protein and does not interact with Parkin.

988 (C) Representative images of HeLa cells probed with antibodies against GRASP65 and GM130. Cells
989 were fixed, permeabilized and incubated with the indicated primary antibodies, corresponding
990 fluorophore-conjugated secondary antibodies, and Hoechst for nuclear staining. GRASP65 is a
991 peripheral membrane protein that resides in the *cis*-Golgi apparatus and interacts with GM130,
992 which is also expressed in the *cis*-Golgi network.

993

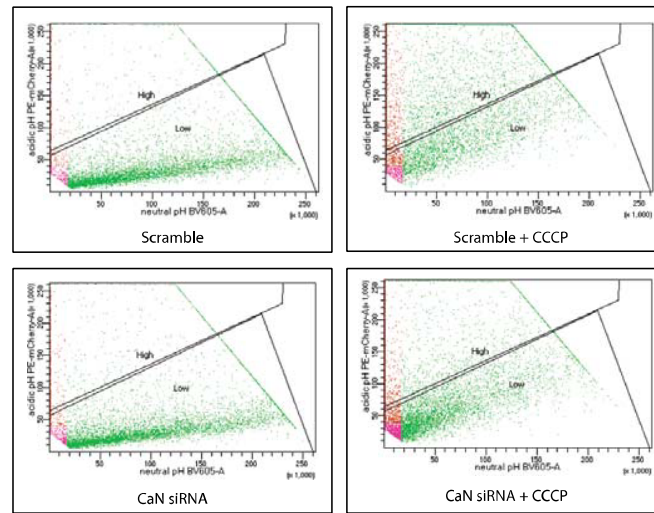


994

995 **Supplementary Figure 7: Calcineurin interacts with Parkin**

996 HEK 293T cells were treated with CCCP-2hrs and subjected to immunoprecipitation (IP) of CaN
997 using anti-CaN antibody. Western Blot analysis was performed with antibody anti-Parkin on the
998 pulled down samples. Inputs represent 5% of the protein lysates and IP eluate 100% of the protein
999 lysates.

1000



1001

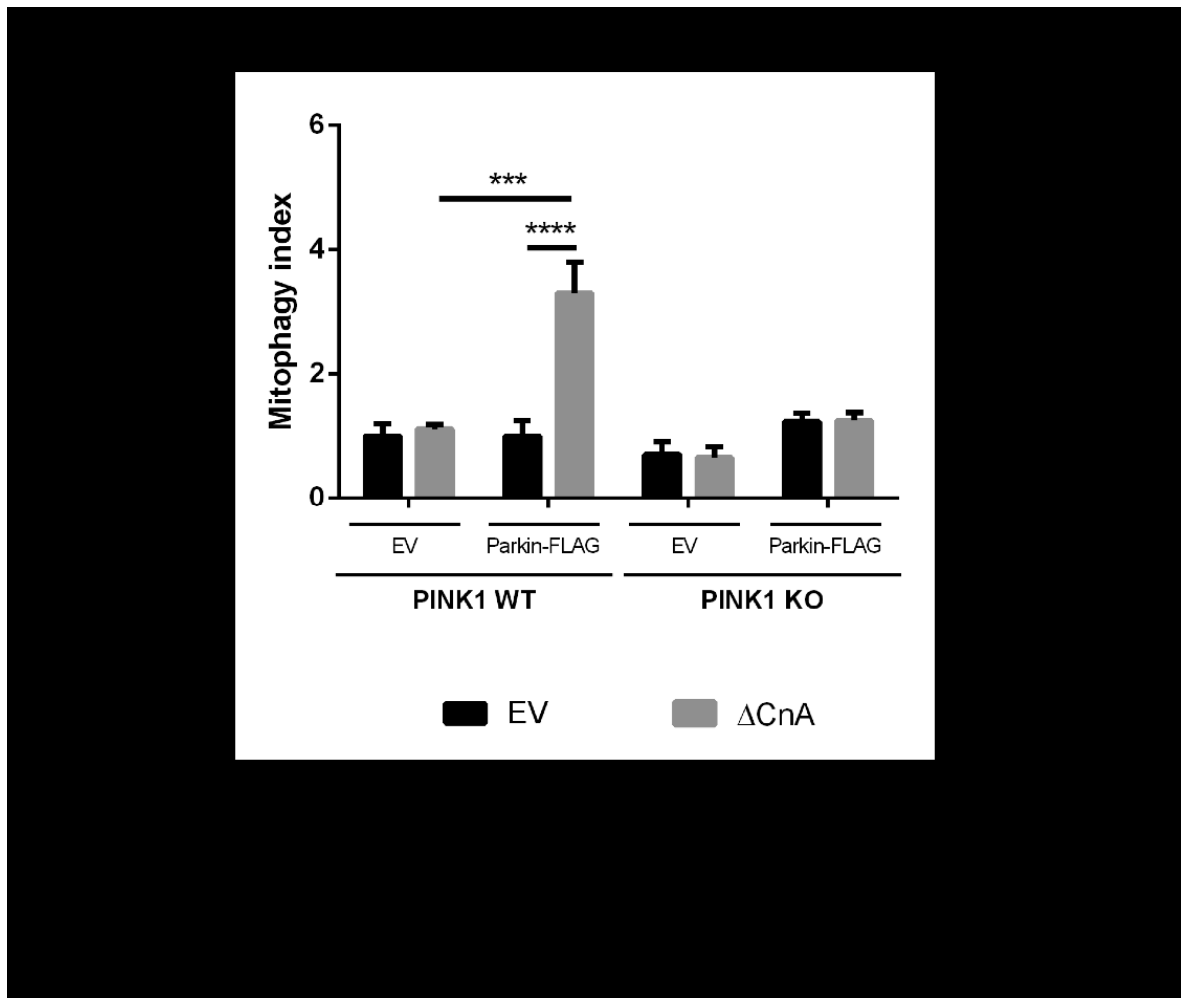
1002 **Supplementary Figure 8: CCCP-induced mitophagy is impaired in cells downregulating**

1003 **Calcineurin**

1004 Representative scatterplots depicting the mean relative level of global mt-Keima signal in CaN

1005 downregulating cells and relative control.

1006



1007

1008

Supplementary Figure 9: CaN-induced mitophagy is mediated by Parkin

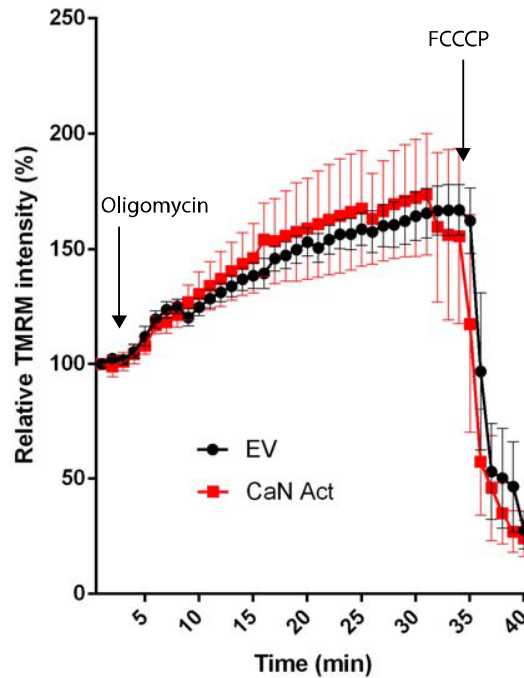
1009 Mt-Keima analysis in MEF cells, which do not express Parkin compared to Parkin-flag expressing

1010 cells. In PINK1 WT background, expression of constitutively active CaN failed to induce mitophagy

1011 in Parkin deficient cells, while the opposite effect was observed in stable cell line expressing

1012 Parkin-Flag. Two-way ANOVA followed by Tukey's multiple comparison test ($n \geq 3$; $p < 0.001$).

1013



1014

1015 **Supplementary Figure 10: Expression of constitutive active Calcineurin does not affect**
1016 **mitochondria membrane potential**

1017 Analysis of mitochondria membrane potential upon expression of constitutive active CaN. MEFs
1018 cells were incubated in presence of 10nM TMRM, and images were acquired with confocal
1019 microscope. Changes of mitochondria TMRM fluorescence (expressed as the % of initial
1020 fluorescence) were followed over time.

1021 REFERENCES

- 1022 1 Moore, D. J., West, A. B., Dawson, V. L. & Dawson, T. M. Molecular pathophysiology of Parkinson's
1023 disease. *Annu Rev Neurosci* **28**, 57-87 (2005).
- 1024 2 Samii, A., Nutt, J. G. & Ransom, B. R. Parkinson's disease. *Lancet* **363**, 1783-1793,
1025 doi:10.1016/S0140-6736(04)16305-8 (2004).
- 1026 3 Spillantini, M. G. *et al.* Alpha-synuclein in Lewy bodies. *Nature* **388**, 839-840, doi:10.1038/42166
1027 (1997).
- 1028 4 Dauer, W. & Przedborski, S. Parkinson's disease: mechanisms and models. *Neuron* **39**, 889-909,
1029 doi:10.1016/s0896-6273(03)00568-3 (2003).
- 1030 5 Narendra, D., Walker, J. E. & Youle, R. Mitochondrial quality control mediated by PINK1 and Parkin:
1031 links to parkinsonism. *Cold Spring Harb Perspect Biol* **4**, doi:10.1101/cshperspect.a011338 (2012).
- 1032 6 Greenamyre, J. T., MacKenzie, G., Peng, T. I. & Stephans, S. E. Mitochondrial dysfunction in
1033 Parkinson's disease. *Biochem Soc Symp* **66**, 85-97 (1999).
- 1034 7 Gasser, T. Molecular pathogenesis of Parkinson disease: insights from genetic studies. *Expert Rev*
1035 *Mol Med* **11**, e22 (2009).
- 1036 8 Shulman, J. M., De Jager, P. L. & Feany, M. B. Parkinson's disease: genetics and pathogenesis. *Annu*
1037 *Rev Pathol* **6**, 193-222, doi:10.1146/annurev-pathol-011110-130242 (2011).
- 1038 9 Valente, E. M. *et al.* Hereditary early-onset Parkinson's disease caused by mutations in PINK1.
1039 *Science* **304**, 1158-1160, doi:10.1126/science.1096284
- 1040 1096284 [pii] (2004).
- 1041 10 Valente, E. M. *et al.* PINK1 mutations are associated with sporadic early-onset parkinsonism. *Annals*
1042 *of neurology* **56**, 336-341, doi:10.1002/ana.20256 (2004).
- 1043 11 Kitada, T. *et al.* Mutations in the parkin gene cause autosomal recessive juvenile parkinsonism.
1044 *Nature* **392**, 605-608, doi:10.1038/33416 (1998).
- 1045 12 Tanaka, K., Suzuki, T. & Chiba, T. The ligation systems for ubiquitin and ubiquitin-like proteins. *Mol*
1046 *Cells* **8**, 503-512 (1998).
- 1047 13 Trempe, J. F. *et al.* Structure of parkin reveals mechanisms for ubiquitin ligase activation. *Science*
1048 **340**, 1451-1455, doi:10.1126/science.1237908 (2013).
- 1049 14 Dove, K. K. & Klevit, R. E. Structural Biology: Parkin's Serpentine Shape Revealed in the Year of the
1050 Snake. *Curr Biol* **23**, R691-693, doi:10.1016/j.cub.2013.07.039 (2013).
- 1051 15 Seirafi, M., Kozlov, G. & Gehring, K. Parkin structure and function. *The FEBS journal* **282**, 2076-2088,
1052 doi:10.1111/febs.13249 (2015).
- 1053 16 Wauer, T. & Komander, D. Structure of the human Parkin ligase domain in an autoinhibited state.
1054 *EMBO J* **32**, 2099-2112, doi:10.1038/emboj.2013.125 (2013).
- 1055 17 Dorn, G. W., 2nd. Central Parkin: The evolving role of Parkin in the heart. *Biochim Biophys Acta*
1056 **1857**, 1307-1312, doi:10.1016/j.bbabi.2016.03.014 (2016).
- 1057 18 Zhang, C. W., Hang, L., Yao, T. P. & Lim, K. L. Parkin Regulation and Neurodegenerative Disorders.
1058 *Front Aging Neurosci* **7**, 248, doi:10.3389/fnagi.2015.00248 (2015).
- 1059 19 Winklhofer, K. F. Parkin and mitochondrial quality control: toward assembling the puzzle. *Trends*
1060 *Cell Biol* **24**, 332-341, doi:10.1016/j.tcb.2014.01.001 (2014).
- 1061 20 Yang, H., Zhou, H. Y., Li, B. & Chen, S. D. Neuroprotection of Parkin against apoptosis is independent
1062 of inclusion body formation. *Neuroreport* **16**, 1117-1121, doi:10.1097/00001756-200507130-00017
1063 (2005).
- 1064 21 Yasuda, T. *et al.* Parkin-mediated protection of dopaminergic neurons in a chronic MPTP-minipump
1065 mouse model of Parkinson disease. *J Neuropathol Exp Neurol* **70**, 686-697,
1066 doi:10.1097/NEN.0b013e3182269ecd (2011).
- 1067 22 Trempe, J. F. & Fon, E. A. Structure and Function of Parkin, PINK1, and DJ-1, the Three Musketeers
1068 of Neuroprotection. *Front Neurol* **4**, 38, doi:10.3389/fneur.2013.00038 (2013).
- 1069 23 Hang, L., Thundiyil, J. & Lim, K. L. Mitochondrial dysfunction and Parkinson disease: a Parkin-AMPK
1070 alliance in neuroprotection. *Ann N Y Acad Sci* **1350**, 37-47, doi:10.1111/nyas.12820 (2015).

- 1071 24 Tanaka, A. Parkin-mediated selective mitochondrial autophagy, mitophagy: Parkin purges damaged
1072 organelles from the vital mitochondrial network. *FEBS Lett* **584**, 1386-1392,
1073 doi:10.1016/j.febslet.2010.02.060 (2010).
- 1074 25 Hampe, C., Ardila-Osorio, H., Fournier, M., Brice, A. & Corti, O. Biochemical analysis of Parkinson's
1075 disease-causing variants of Parkin, an E3 ubiquitin-protein ligase with monoubiquitylation capacity.
1076 *Hum Mol Genet* **15**, 2059-2075, doi:10.1093/hmg/ddl131 (2006).
- 1077 26 Matsuda, N. *et al.* Diverse effects of pathogenic mutations of Parkin that catalyze multiple
1078 monoubiquitylation in vitro. *J Biol Chem* **281**, 3204-3209, doi:10.1074/jbc.M510393200 (2006).
- 1079 27 Durcan, T. M., Kontogiannea, M., Bedard, N., Wing, S. S. & Fon, E. A. Ataxin-3 deubiquitination is
1080 coupled to Parkin ubiquitination via E2 ubiquitin-conjugating enzyme. *J Biol Chem* **287**, 531-541,
1081 doi:10.1074/jbc.M111.288449 (2012).
- 1082 28 Joch, M. *et al.* Parkin-mediated monoubiquitination of the PDZ protein PICK1 regulates the activity
1083 of acid-sensing ion channels. *Mol Biol Cell* **18**, 3105-3118, doi:10.1091/mbc.e05-11-1027 (2007).
- 1084 29 Chen, D. *et al.* Parkin mono-ubiquitinates Bcl-2 and regulates autophagy. *J Biol Chem* **285**, 38214-
1085 38223, doi:10.1074/jbc.M110.101469 (2010).
- 1086 30 Moore, D. J., West, A. B., Dikeman, D. A., Dawson, V. L. & Dawson, T. M. Parkin mediates the
1087 degradation-independent ubiquitination of Hsp70. *Journal of neurochemistry* **105**, 1806-1819,
1088 doi:10.1111/j.1471-4159.2008.05261.x (2008).
- 1089 31 Muller-Rischart, A. K. *et al.* The E3 ligase parkin maintains mitochondrial integrity by increasing
1090 linear ubiquitination of NEMO. *Molecular cell* **49**, 908-921, doi:10.1016/j.molcel.2013.01.036
1091 (2013).
- 1092 32 Narendra, D. P. *et al.* PINK1 is selectively stabilized on impaired mitochondria to activate Parkin.
1093 *PLoS Biol* **8**, e1000298.
- 1094 33 Vives-Bauza, C. *et al.* PINK1-dependent recruitment of Parkin to mitochondria in mitophagy. *Proc*
1095 *Natl Acad Sci U S A* **107**, 378-383, doi:10.1073/pnas.0911187107 (2010).
- 1096 34 Matsuda, N. *et al.* PINK1 stabilized by mitochondrial depolarization recruits Parkin to damaged
1097 mitochondria and activates latent Parkin for mitophagy. *J Cell Biol* **189**, 211-221,
1098 doi:10.1083/jcb.200910140 (2010).
- 1099 35 Lin, W. & Kang, U. J. Characterization of PINK1 processing, stability, and subcellular localization.
1100 *Journal of neurochemistry* **106**, 464-474, doi:10.1111/j.1471-4159.2008.05398.x (2008).
- 1101 36 Jin, S. M. *et al.* Mitochondrial membrane potential regulates PINK1 import and proteolytic
1102 destabilization by PARL. *J Cell Biol* **191**, 933-942, doi:10.1083/jcb.201008084 (2010).
- 1103 37 Yamano, K. & Youle, R. J. PINK1 is degraded through the N-end rule pathway. *Autophagy* **9**, 1758-
1104 1769, doi:10.4161/auto.24633 (2013).
- 1105 38 Ziviani, E., Tao, R. N. & Whitworth, A. J. Drosophila parkin requires PINK1 for mitochondrial
1106 translocation and ubiquitinates mitofusin. *Proc Natl Acad Sci U S A* **107**, 5018-5023,
1107 doi:10.1073/pnas.0913485107 (2010).
- 1108 39 Narendra, D. P. *et al.* PINK1 is selectively stabilized on impaired mitochondria to activate Parkin.
1109 *PLoS Biol* **8**, e1000298, doi:10.1371/journal.pbio.1000298 (2010).
- 1110 40 Kondapalli, C. *et al.* PINK1 is activated by mitochondrial membrane potential depolarization and
1111 stimulates Parkin E3 ligase activity by phosphorylating Serine 65. *Open Biol* **2**, 120080,
1112 doi:10.1098/rsob.120080 (2012).
- 1113 41 Kazlauskaitė, A. *et al.* Parkin is activated by PINK1-dependent phosphorylation of ubiquitin at Ser65.
1114 *Biochem J* **460**, 127-139, doi:10.1042/BJ20140334 (2014).
- 1115 42 Kazlauskaitė, A. *et al.* Phosphorylation of Parkin at Serine65 is essential for activation: elaboration
1116 of a Miro1 substrate-based assay of Parkin E3 ligase activity. *Open Biol* **4**, 130213,
1117 doi:10.1098/rsob.130213 (2014).
- 1118 43 Koyano, F. *et al.* Ubiquitin is phosphorylated by PINK1 to activate parkin. *Nature* **510**, 162-166,
1119 doi:10.1038/nature13392 (2014).
- 1120 44 Yoshii, S. R., Kishi, C., Ishihara, N. & Mizushima, N. Parkin mediates proteasome-dependent protein
1121 degradation and rupture of the outer mitochondrial membrane. *J Biol Chem* **286**, 19630-19640,
1122 doi:10.1074/jbc.M110.209338 (2011).

- 1123 45 Chan, N. C. *et al.* Broad activation of the ubiquitin-proteasome system by Parkin is critical for
1124 mitophagy. *Hum Mol Genet* **20**, 1726-1737, doi:10.1093/hmg/ddr048 (2011).
- 1125 46 Narendra, D., Tanaka, A., Suen, D. F. & Youle, R. J. Parkin is recruited selectively to impaired
1126 mitochondria and promotes their autophagy. *J Cell Biol* **183**, 795-803 (2008).
- 1127 47 Tanaka, A. *et al.* Proteasome and p97 mediate mitophagy and degradation of mitofusins induced by
1128 Parkin. *J Cell Biol* **191**, 1367-1380, doi:10.1083/jcb.201007013 (2010).
- 1129 48 Sarraf, S. A. *et al.* Landscape of the PARKIN-dependent ubiquitylome in response to mitochondrial
1130 depolarization. *Nature* **496**, 372-376, doi:10.1038/nature12043 (2013).
- 1131 49 Chen, Y. & Dorn, G. W., 2nd. PINK1-phosphorylated mitofusin 2 is a Parkin receptor for culling
1132 damaged mitochondria. *Science* **340**, 471-475, doi:10.1126/science.1231031 (2013).
- 1133 50 Ashrafi, G. & Schwarz, T. L. The pathways of mitophagy for quality control and clearance of
1134 mitochondria. *Cell Death Differ* **20**, 31-42, doi:10.1038/cdd.2012.81 (2013).
- 1135 51 Pryde, K. R., Smith, H. L., Chau, K. Y. & Schapira, A. H. PINK1 disables the anti-fission machinery to
1136 segregate damaged mitochondria for mitophagy. *J Cell Biol* **213**, 163-171,
1137 doi:10.1083/jcb.201509003 (2016).
- 1138 52 Cereghetti, G. M. *et al.* Dephosphorylation by calcineurin regulates translocation of Drp1 to
1139 mitochondria. *Proc Natl Acad Sci U S A* **105**, 15803-15808, doi:10.1073/pnas.0808249105 (2008).
- 1140 53 Han, H. *et al.* PINK1 phosphorylates Drp1(S616) to regulate mitophagy-independent mitochondrial
1141 dynamics. *EMBO Rep* **21**, e48686, doi:10.15252/embr.201948686 (2020).
- 1142 54 Buhlman, L. *et al.* Functional interplay between Parkin and Drp1 in mitochondrial fission and
1143 clearance. *Biochim Biophys Acta* **1843**, 2012-2026, doi:10.1016/j.bbamcr.2014.05.012 (2014).
- 1144 55 Burman, J. L. *et al.* Mitochondrial fission facilitates the selective mitophagy of protein aggregates. *J*
1145 *Cell Biol* **216**, 3231-3247, doi:10.1083/jcb.201612106 (2017).
- 1146 56 Kanki, T. *et al.* A genomic screen for yeast mutants defective in selective mitochondria autophagy.
1147 *Mol Biol Cell* **20**, 4730-4738, doi:10.1091/mbc.E09-03-0225 (2009).
- 1148 57 Pereira, M. B. *et al.* Carbonyl cyanide m-chlorophenylhydrazone induced calcium signaling and
1149 activation of plasma membrane H(+)-ATPase in the yeast *Saccharomyces cerevisiae*. *FEMS yeast*
1150 *research* **8**, 622-630, doi:10.1111/j.1567-1364.2008.00380.x (2008).
- 1151 58 Twig, G. *et al.* Fission and selective fusion govern mitochondrial segregation and elimination by
1152 autophagy. *EMBO J* **27**, 433-446, doi:7601963 [pii]
1153 10.1038/sj.emboj.7601963 (2008).
- 1154 59 Twig, G. & Shirihai, O. S. The interplay between mitochondrial dynamics and mitophagy.
1155 *Antioxidants & redox signaling* **14**, 1939-1951, doi:10.1089/ars.2010.3779 (2011).
- 1156 60 Medina, D. L. *et al.* Lysosomal calcium signalling regulates autophagy through calcineurin and TFEB.
1157 *Nat Cell Biol* **17**, 288-299, doi:10.1038/ncb3114 (2015).
- 1158 61 Okatsu, K. *et al.* p62/SQSTM1 cooperates with Parkin for perinuclear clustering of depolarized
1159 mitochondria. *Genes Cells* **15**, 887-900, doi:10.1111/j.1365-2443.2010.01426.x (2010).
- 1160 62 Rizk, A. *et al.* Segmentation and quantification of subcellular structures in fluorescence microscopy
1161 images using Squassh. *Nature protocols* **9**, 586-596, doi:10.1038/nprot.2014.037 (2014).
- 1162 63 Friberg, H., Ferrand-Drake, M., Bengtsson, F., Halestrap, A. P. & Wieloch, T. Cyclosporin A, but not
1163 FK 506, protects mitochondria and neurons against hypoglycemic damage and implicates the
1164 mitochondrial permeability transition in cell death. *J Neurosci* **18**, 5151-5159 (1998).
- 1165 64 Zou, Y. *et al.* Calcineurin plays a critical role in the development of pressure overload-induced
1166 cardiac hypertrophy. *Circulation* **104**, 97-101, doi:10.1161/01.cir.104.1.97 (2001).
- 1167 65 Zou, Y. *et al.* Isoproterenol activates extracellular signal-regulated protein kinases in
1168 cardiomyocytes through calcineurin. *Circulation* **104**, 102-108, doi:10.1161/hc2601.090987 (2001).
- 1169 66 Chaugule, V. K. *et al.* Autoregulation of Parkin activity through its ubiquitin-like domain. *EMBO J* **30**,
1170 2853-2867, doi:10.1038/emboj.2011.204 (2011).
- 1171 67 Riley, B. E. *et al.* Structure and function of Parkin E3 ubiquitin ligase reveals aspects of RING and
1172 HECT ligases. *Nature communications* **4**, 1982, doi:10.1038/ncomms2982 (2013).
- 1173 68 Spratt, D. E. *et al.* A molecular explanation for the recessive nature of parkin-linked Parkinson's
1174 disease. *Nature communications* **4**, 1983, doi:10.1038/ncomms2983 (2013).

- 1175 69 Kane, L. A. *et al.* PINK1 phosphorylates ubiquitin to activate Parkin E3 ubiquitin ligase activity. *J Cell Biol* **205**, 143-153, doi:10.1083/jcb.201402104 (2014).
1176
1177 70 Kumar, A. *et al.* Disruption of the autoinhibited state primes the E3 ligase parkin for activation and
1178 catalysis. *EMBO J* **34**, 2506-2521, doi:10.15252/embj.201592337 (2015).
1179 71 Ishii, T. *et al.* CETSA quantitatively verifies in vivo target engagement of novel RIPK1 inhibitors in
1180 various biospecimens. *Scientific reports* **7**, 13000, doi:10.1038/s41598-017-12513-1 (2017).
1181 72 Jafari, R. *et al.* The cellular thermal shift assay for evaluating drug target interactions in cells. *Nature*
1182 *protocols* **9**, 2100-2122, doi:10.1038/nprot.2014.138 (2014).
1183 73 Barr, F. A., Nakamura, N. & Warren, G. Mapping the interaction between GRASP65 and GM130,
1184 components of a protein complex involved in the stacking of Golgi cisternae. *EMBO J* **17**, 3258-
1185 3268, doi:10.1093/emboj/17.12.3258 (1998).
1186 74 Ayala, I., Crispino, R. & Colanzi, A. GRASP65 controls Golgi position and structure during G2/M
1187 transition by regulating the stability of microtubules. *Traffic* **20**, 785-802, doi:10.1111/tra.12682
1188 (2019).
1189 75 Lee, J. Y., Nagano, Y., Taylor, J. P., Lim, K. L. & Yao, T. P. Disease-causing mutations in parkin impair
1190 mitochondrial ubiquitination, aggregation, and HDAC6-dependent mitophagy. *J Cell Biol* **189**, 671-
1191 679, doi:jcb.201001039 [pii]
1192 10.1083/jcb.201001039.
1193 76 Ding, W. X. *et al.* Nix is critical to two distinct phases of mitophagy, reactive oxygen species-
1194 mediated autophagy induction and Parkin-ubiquitin-p62-mediated mitochondrial priming. *J Biol*
1195 *Chem* **285**, 27879-27890, doi:10.1074/jbc.M110.119537 (2010).
1196 77 Ding, W. X. *et al.* Parkin and mitofusins reciprocally regulate mitophagy and mitochondrial spheroid
1197 formation. *J Biol Chem* **287**, 42379-42388, doi:10.1074/jbc.M112.413682 (2012).
1198 78 Lee, J. Y., Nagano, Y., Taylor, J. P., Lim, K. L. & Yao, T. P. Disease-causing mutations in parkin impair
1199 mitochondrial ubiquitination, aggregation, and HDAC6-dependent mitophagy. *J Cell Biol* **189**, 671-
1200 679, doi:10.1083/jcb.201001039 (2010).
1201 79 Geisler, S. *et al.* PINK1/Parkin-mediated mitophagy is dependent on VDAC1 and p62/SQSTM1. *Nat*
1202 *Cell Biol* **12**, 119-131, doi:10.1038/ncb2012 (2010).
1203 80 Chan, N. C. & Chan, D. C. Parkin uses the UPS to ship off dysfunctional mitochondria. *Autophagy* **7**,
1204 771-772, doi:10.4161/auto.7.7.15453 (2011).
1205 81 Kitamura, T. *et al.* Retrovirus-mediated gene transfer and expression cloning: powerful tools in
1206 functional genomics. *Exp Hematol* **31**, 1007-1014 (2003).
1207 82 Katayama, H., Kogure, T., Mizushima, N., Yoshimori, T. & Miyawaki, A. A sensitive and quantitative
1208 technique for detecting autophagic events based on lysosomal delivery. *Chem Biol* **18**, 1042-1052,
1209 doi:10.1016/j.chembiol.2011.05.013 (2011).
1210 83 Sugiura, A. *et al.* MITOL regulates endoplasmic reticulum-mitochondria contacts via Mitofusin2.
1211 *Molecular cell* **51**, 20-34, doi:10.1016/j.molcel.2013.04.023 (2013).
1212 84 Yun, J. *et al.* MUL1 acts in parallel to the PINK1/parkin pathway in regulating mitofusin and
1213 compensates for loss of PINK1/parkin. *eLife* **3**, e01958, doi:10.7554/eLife.01958 (2014).
1214 85 Poole, A. C. *et al.* The PINK1/Parkin pathway regulates mitochondrial morphology. *Proc Natl Acad Sci U S A* **105**,
1215 1638-1643 (2008).
1216 86 Clark, I. E. *et al.* Drosophila pink1 is required for mitochondrial function and interacts genetically
1217 with parkin. *Nature* **441**, 1162-1166 (2006).
1218 87 Park, J. *et al.* Mitochondrial dysfunction in Drosophila PINK1 mutants is complemented by parkin.
1219 *Nature* **441**, 1157-1161 (2006).
1220 88 Yang, Y. *et al.* Mitochondrial pathology and muscle and dopaminergic neuron degeneration caused
1221 by inactivation of Drosophila Pink1 is rescued by Parkin. *Proc Natl Acad Sci U S A* **103**, 10793-10798
1222 (2006).
1223 89 Chakraborty, J. *et al.* USP14 inhibition corrects an in vivo model of impaired mitophagy. *EMBO*
1224 *molecular medicine* **10**, doi:10.15252/emmm.201809014 (2018).
1225 90 von Stockum, S. *et al.* Inhibition of the deubiquitinase USP8 corrects a Drosophila PINK1 model of
1226 mitochondria dysfunction. *Life Sci Alliance* **2**, doi:10.26508/lsa.201900392 (2019).

- 1227 91 Lee, J. J. *et al.* Basal mitophagy is widespread in *Drosophila* but minimally affected by loss of Pink1
1228 or parkin. *J Cell Biol* **217**, 1613-1622, doi:10.1083/jcb.201801044 (2018).
- 1229 92 Cornelissen, T. *et al.* Deficiency of parkin and PINK1 impairs age-dependent mitophagy in
1230 *Drosophila*. *eLife* **7**, doi:10.7554/eLife.35878 (2018).
- 1231 93 Vives-Bauza, C., de Vries, R. L., Tocilescu, M. & Przedborski, S. PINK1/Parkin direct mitochondria to
1232 autophagy. *Autophagy* **6**, 315-316, doi:11199 [pii].
- 1233 94 Shimura, H. *et al.* Familial Parkinson disease gene product, parkin, is a ubiquitin-protein ligase. *Nat*
1234 *Genet* **25**, 302-305 (2000).
- 1235 95 Sha, D., Chin, L. S. & Li, L. Phosphorylation of parkin by Parkinson disease-linked kinase PINK1
1236 activates parkin E3 ligase function and NF-kappaB signaling. *Hum Mol Genet* **19**, 352-363,
1237 doi:10.1093/hmg/ddp501 (2010).
- 1238 96 Wang, X. *et al.* PINK1 and Parkin target Miro for phosphorylation and degradation to arrest
1239 mitochondrial motility. *Cell* **147**, 893-906, doi:10.1016/j.cell.2011.10.018 (2011).
- 1240 97 Zhang, C. *et al.* PINK1 triggers autocatalytic activation of Parkin to specify cell fate decisions. *Curr*
1241 *Biol* **24**, 1854-1865, doi:10.1016/j.cub.2014.07.014 (2014).
- 1242 98 Gegg, M. E. *et al.* Mitofusin 1 and mitofusin 2 are ubiquitinated in a PINK1/parkin-dependent
1243 manner upon induction of mitophagy. *Hum Mol Genet* **19**, 4861-4870, doi:10.1093/hmg/ddq419
1244 (2010).
- 1245 99 Poole, A. C., Thomas, R. E., Yu, S., Vincow, E. S. & Pallanck, L. The mitochondrial fusion-promoting
1246 factor mitofusin is a substrate of the PINK1/parkin pathway. *PLoS One* **5**, e10054,
1247 doi:10.1371/journal.pone.0010054 (2010).
- 1248 100 Bjorkoy, G. *et al.* p62/SQSTM1 forms protein aggregates degraded by autophagy and has a
1249 protective effect on huntingtin-induced cell death. *J Cell Biol* **171**, 603-614,
1250 doi:10.1083/jcb.200507002 (2005).
- 1251 101 Lee, J. Y. *et al.* HDAC6 controls autophagosome maturation essential for ubiquitin-selective quality-
1252 control autophagy. *EMBO J* **29**, 969-980, doi:10.1038/emboj.2009.405 (2010).
- 1253 102 von Muhlinen, N., Thurston, T., Ryzhakov, G., Bloor, S. & Randow, F. NDP52, a novel autophagy
1254 receptor for ubiquitin-decorated cytosolic bacteria. *Autophagy* **6**, 288-289,
1255 doi:10.4161/auto.6.2.11118 (2010).
- 1256 103 Jin, S. M. & Youle, R. J. The accumulation of misfolded proteins in the mitochondrial matrix is
1257 sensed by PINK1 to induce PARK2/Parkin-mediated mitophagy of polarized mitochondria.
1258 *Autophagy* **9**, 1750-1757, doi:10.4161/auto.26122 (2013).
- 1259 104 Yu, Z. *et al.* Mitochondrial Ca²⁺ oscillation induces mitophagy initiation through the PINK1-Parkin
1260 pathway. *Cell Death Dis* **12**, 632, doi:10.1038/s41419-021-03913-3 (2021).
- 1261 105 Kubli, D. A. *et al.* PINK1 Is Dispensable for Mitochondrial Recruitment of Parkin and Activation of
1262 Mitophagy in Cardiac Myocytes. *PLoS One* **10**, e0130707, doi:10.1371/journal.pone.0130707
1263 (2015).
- 1264 106 Lee, S. B. *et al.* The AMPK-Parkin axis negatively regulates necroptosis and tumorigenesis by
1265 inhibiting the necrosome. *Nat Cell Biol* **21**, 940-951, doi:10.1038/s41556-019-0356-8 (2019).
- 1266 107 Avraham, E., Rott, R., Liani, E., Szargel, R. & Engelender, S. Phosphorylation of Parkin by the cyclin-
1267 dependent kinase 5 at the linker region modulates its ubiquitin-ligase activity and aggregation. *J*
1268 *Biol Chem* **282**, 12842-12850, doi:10.1074/jbc.M608243200 (2007).
- 1269 108 Lee, S. B. *et al.* Parkin Regulates Mitosis and Genomic Stability through Cdc20/Cdh1. *Molecular cell*
1270 **60**, 21-34, doi:10.1016/j.molcel.2015.08.011 (2015).
- 1271 109 Hung, C. M. *et al.* AMPK/ULK1-mediated phosphorylation of Parkin ACT domain mediates an early
1272 step in mitophagy. *Sci Adv* **7**, doi:10.1126/sciadv.abg4544 (2021).
- 1273 110 Balasubramaniam, M. *et al.* Interleukin-1beta drives NEDD8 nuclear-to-cytoplasmic translocation,
1274 fostering parkin activation via NEDD8 binding to the P-ubiquitin activating site. *J*
1275 *Neuroinflammation* **16**, 275, doi:10.1186/s12974-019-1669-z (2019).
- 1276 111 Um, J. W. *et al.* Neddylation positively regulates the ubiquitin E3 ligase activity of parkin. *J Neurosci*
1277 *Res* **90**, 1030-1042, doi:10.1002/jnr.22828 (2012).

- 1278 112 McLelland, G. L., Soubannier, V., Chen, C. X., McBride, H. M. & Fon, E. A. Parkin and PINK1 function
1279 in a vesicular trafficking pathway regulating mitochondrial quality control. *EMBO J* **33**, 282-295,
1280 doi:10.1002/embj.201385902 (2014).
- 1281 113 McLelland, G. L., Lee, S. A., McBride, H. M. & Fon, E. A. Syntaxin-17 delivers PINK1/parkin-
1282 dependent mitochondrial vesicles to the endolysosomal system. *J Cell Biol* **214**, 275-291,
1283 doi:10.1083/jcb.201603105 (2016).
- 1284 114 Towers, C. G. *et al.* Mitochondrial-derived vesicles compensate for loss of LC3-mediated mitophagy.
1285 *Dev Cell* **56**, 2029-2042 e2025, doi:10.1016/j.devcel.2021.06.003 (2021).
- 1286 115 Koentjoro, B., Park, J. S. & Sue, C. M. Nix restores mitophagy and mitochondrial function to protect
1287 against PINK1/Parkin-related Parkinson's disease. *Scientific reports* **7**, 44373,
1288 doi:10.1038/srep44373 (2017).
- 1289 116 Morais, V. A. *et al.* PINK1 loss-of-function mutations affect mitochondrial complex I activity via
1290 Ndufa10 ubiquinone uncoupling. *Science* **344**, 203-207, doi:10.1126/science.1249161 (2014).
- 1291 117 Matheoud, D. *et al.* Parkinson's Disease-Related Proteins PINK1 and Parkin Repress Mitochondrial
1292 Antigen Presentation. *Cell* **166**, 314-327, doi:10.1016/j.cell.2016.05.039 (2016).
- 1293 118 Cecconi, C., Shank, E. A., Bustamante, C. & Marqusee, S. Direct observation of the three-state
1294 folding of a single protein molecule. *Science* **309**, 2057-2060, doi:10.1126/science.1116702 (2005).
- 1295 119 Costa, V. *et al.* Mitochondrial fission and cristae disruption increase the response of cell models of
1296 Huntington's disease to apoptotic stimuli. *EMBO molecular medicine* **2**, 490-503,
1297 doi:10.1002/emmm.201000102 (2010).
- 1298 120 Um, J. H., Kim, Y. Y., Finkel, T. & Yun, J. Sensitive Measurement of Mitophagy by Flow Cytometry
1299 Using the pH-dependent Fluorescent Reporter mt-Keima. *Journal of visualized experiments : JoVE*,
1300 doi:10.3791/58099 (2018).
- 1301 121 Minisini, M. *et al.* Transcriptomic and genomic studies classify NKL54 as a histone deacetylase
1302 inhibitor with indirect influence on MEF2-dependent transcription. *Nucleic Acids Res* **50**, 2566-
1303 2586, doi:10.1093/nar/gkac081 (2022).
- 1304 122 Dijkers, P. F. & O'Farrell, P. H. Drosophila calcineurin promotes induction of innate immune
1305 responses. *Curr Biol* **17**, 2087-2093, doi:10.1016/j.cub.2007.11.001 (2007).
- 1306 123 Montava-Garriga, L., Singh, F., Ball, G. & Ganley, I. G. Semi-automated quantitation of mitophagy in
1307 cells and tissues. *Mech Ageing Dev* **185**, 111196, doi:10.1016/j.mad.2019.111196 (2020).
- 1308 124 Chakraborty, J., Caicci, F., Roy, M. & Ziviani, E. Investigating mitochondrial autophagy by routine
1309 transmission electron microscopy: Seeing is believing? *Pharmacol Res* **160**, 105097,
1310 doi:10.1016/j.phrs.2020.105097 (2020).
- 1311 125 Duchen, M. R. Mitochondria and calcium: from cell signalling to cell death. *J Physiol* **529 Pt 1**, 57-68,
1312 doi:10.1111/j.1469-7793.2000.00057.x (2000).
- 1313 126 Klee, C. B., Crouch, T. H. & Krinks, M. H. Calcineurin: a calcium- and calmodulin-binding protein of
1314 the nervous system. *Proc Natl Acad Sci U S A* **76**, 6270-6273, doi:10.1073/pnas.76.12.6270 (1979).
- 1315